universität wien

MASTERARBEIT / MASTER'S THESIS

Titel der Masterarbeit / Title of the Master's Thesis

„Investigating Metabolic Implications of MEK1"

verfasst von / submitted by

Michael A. Bryant

angestrebter akademischer Grad / in partial fulfilment of the requirements for the degree of

Master of Science (MSc)

Wien, 2021 / Vienna 2021

Studienkennzahl lt. Studienblatt / degree programme code as it appears on the student record sheet:	UA 066 606
Studienrichtung lt. Studienblatt / degree programme as it appears on the student record sheet:	Masterstudium Drug Discovery and Development
Betreut von / Supervisor:	Prof. Dr. Manuela Baccarini, PhD

Acknowledgments

Through a year of uncertainties, in world where we planned to unplan things held dear, I am most grateful to have had the opportunity to complete my master studies amongst scientists and friends who motivated me to question, to learn, and ultimately, to succeed. Foremost I give my thanks to Georg Vucak, for inviting me to the engaging environment of the Baccarini lab and supporting me throughout my thesis project. I enjoyed the comradery from all members of the Baccarini lab. Specifically, I want to thank Stefanie Toifl for her endless knowledge of cell biology and her solicitous advice. Moreover, I must give my utmost thanks to Professor Manuela Baccarini for the opportunity she provided me. Through all of my academic pursuits, I have never been more inspired by a professor. I greatly appreciate our discussions that evoked my scientific curiosity and the time Manuela took to support me in my project.

As the project began investigating protein neighborhoods, I would like to thank the neighboring Decker, Kovarik, and Versteeg labs. My sincere gratitude and thanks go out to a most special neighbor, Duygu Demiröz-Bas. Duygu was not only an excellent scientific mentor, but is also a caring and wonderful friend. I cherish the memories and laughs we shared on the bench together and the toasts we made to the successful (and unsuccessful) experiments. Duygu truly enriched my experience at the Max Perutz Labs, and for that I am ever grateful.

An ocean away, I want to thank my family for their continuous support in all my life decisions. After two years of phone calls and video chats, I revel at the opportunity to be reunited once again. Unaffected by the distance of this trying year, I appreciate so the unending love I receive that helps shape and form the person I am and continue to be.

Zusammenfassung

Die Extrazelluläre Signal-regulierte Kinase (ERK) wurde als Hauptregulator des Zelllebens, der Proliferation und des Zellschicksals beschrieben und ist das letzte Protein des kanonischen MAP-Kinase-Weges (MAPK). Die Untersuchung der Komponenten, die der ERK vorausgehen, ist essentiell, um die Integration der MAPK-Signalgebung mit anderen kritischen Signalwegen besser zu verstehen. MEK ist das vorletzte Protein in der MAPK-Signalkaskade und ist für die Regulierung der ERK-Aktivierung verantwortlich. Daher wird die Vertiefung unseres Wissens über die MEK-Aktivität nicht nur unser Verständnis des MAPK-Signalweges als Ganzes bereichern, sondern möglicherweise auch "moonlighting"-Funktionen von MEK1 außerhalb des MAPK-Signalweges beleuchten.

In dieser Studie nutzten wir die Ergebnisse eines kürzlich durchgeführten Proximity-Dependent Labeling Screen, der Interaktoren verschiedener Mutationen von MEK1 untersuchte. Basierend auf den Screen-Ergebnissen wollten wir die metabolischen Implikationen von MEK1-Mutationen und vollständiger MEK1-Ablation untersuchen. Dazu verwendeten wir einen Agilent Seahorse Flux Analyzer, um die Raten der oxidativen Phosphorylierung und der Glykolyse zu vergleichen. Des Weiteren versuchten wir, die Masse, Funktionalität und ROS-Produktion der Mitochondrien in den verschiedenen MEK1-Mutationen mittels Durchflusszytometrie zu bestimmen. Die Ergebnisse zeigten zwar keine signifikanten Unterschiede zwischen den mutierten Formen von MEK1 und MEK1 WT, aber sie zeigten, dass die Ablation von MEK1 mit Veränderungen des Stoffwechsels und der Funktionalität der Mitochondrien korreliert ist. Da Wirkstoffe, die auf den Stoffwechsel abzielen, ein immer relevanteres Thema in der Onkologie werden, ist es interessant, das Zusammenspiel zwischen dem Stoffwechsel und den Schlüsselkomponenten des MAPK-Signalwegs weiter zu entschlüsseln.

Abstract

The Extracellular Signal-Regulated Kinase (ERK) has been described as a master regulator of cell life, proliferation and fate, and is the final tier in the canonical Mitogen-Activated Protein Kinase (MAPK) cascade. Investigations of the components preceding ERK is essential to better understand the integration of MAPK signaling with other critical signaling pathways. MEK is the penultimate player in MAPK signaling and is responsible for regulating ERK activation. As such, deepening our knowledge of MEK activity will not only enrich our understanding of the MAPK pathway as a whole, but also potentially uncover moonlighting functions of MEK1 outside of the MAPK pathway.

In this study, we used the results of a recent proximity dependent labeling screen that assessed interactors of various mutations of MEK1. Based on the screen results, we wanted to investigate metabolic implications of MEK1 mutations and MEK1 ablation. To do this, we used an Agilent Seahorse flux analyzer to compare rates of oxidative phosphorylation and glycolysis. We further endeavored to assess mitochondria mass, functionality, and ROS production in the different variations of MEK1 using flow cytometry. While the results did not imply significant differences between mutant forms of MEK1 and MEK1 WT, it did show that ablating MEK1 is correlated to alterations in metabolism and mitochondria functionality. As therapeutic compounds targeting metabolism becomes an evermore exciting topic in the field of oncology, it proves interesting to further unravel the interplay between metabolism and key components of the MAPK pathway.

Table of Contents

1. Abbreviations

ATP, Adenosine Triphosphate

CCCP, Carbonyl Cyanide m-Chlorophenyl Hydrazone

DOX, Doxycycline

ECAR, Extra Cellular Acidification Rate

EGF, Epidermal Growth Factor

ER, Endoplasmic Reticulum

ERK, Extracellular signal-Regulated Kinase

ETC, Electron Transport Chain

FAO, Fatty Acid Oxidation

FAS, Fatty Acid Synthesis

FCCP, Carbonyl cyanide-*p*-trifluoromethoxyphenylhydrazone

GFP, Green Fluorescent Protein

GPCR, G-Protein Coupled Receptor

IMM, Inner Mitochondrial Membrane

KO, Knock Out

LDHA, Lactate Dehydrogenase A

MAPK, Mitogen-Activated Protein Kinase

MEK, MAPK/ERK Kinase

MNK, MAPK-interacting Kinase

MP1, Scaffold Protein MEK Partner 1

MS, Mass Spectrometry

MSK, Mitogen-Stress associated Kinase

mtDNA, Mitochondrial DNA

NT, Non-treated

OCR, Oxygen Consumption Rate

OXPHOS, Oxidative Phosphorylation

PDL, Proximity Dependent Labeling

PPI, Protein-Protein Interaction

PPP, Pentose Phosphate Pathway

PTEN, Phosphatase Tensin Homolog

PYi, Pyruvate Uptake Inhibitor

RAF, Rapidly Accelerated Fibrosarcoma

RAS, Rat Sarcoma

RDS,RAF Dependent Sites

ROS, Reactive Oxidative Species

RSK, Ribosomal S6 Kinase

RTK, Receptor Tyrosine Kinase

SOS, Son of Sevenless

SRC, Spare Respiratory Capacity

TCA, Tricarboxylic Acid

WT, Wild Type

2. Introduction

2.1 MAPK

As the river Styx was prophesized to bridge the divide between the living and the underworld, another cascade, one of molecular origin, proves to be more than fallacy, instead a bona fide gatekeeper between life and death. The Mitogen-Activated Protein Kinase (MAPK) cascade, and more specifically the ultimate Extracellular signal-Regulated Kinase (ERK), has been described as a master regulator of cell life, behavior, and fate (Lavoie et al., 2020).

Maintaining the critical balance between cell survival, proliferation, migration, and metabolism requires dynamic regulation via both intracellular and extracellular signaling. Intracellular signaling relies heavily on phosphorylation activity, resulting in activation and deactivation of critical nodes in signaling pathways. Extracellular signals, such as cytokines, mitogens, and growth factors, relay information intercellularly, allowing cells to communicate information that ultimately regulates the transcription of genes essential to the specific cellular response (Aaronson, 1991). The interplay of these extracellular signals with intracellular signaling pathways can be visualized and described as a cascade. Just as the water of a river swiftly flows downstream, polishing stone after stone in its wake, so too flows signaling information within the cell. Similar to the discrete placement of the stones in a river, the nodes of protein cascades are conserved and specifically ordered. One protein cascade can induce a variety of downstream targets, thus the tight regulation of these signaling pathways is essential for optimal cell signaling.

Activation of the canonical MAPK pathway begins when various extracellular signaling ligands, including growth factors, cytokines, and mitogens, bind to G-Protein Coupled Receptors (GPCRs) or Receptor Tyrosine Kinases (RTKs). The canonical example of ligands binding to RTKs leads to the dimerization of two receptor subunits, inducing intracellular autophosphorylation of the tyrosine residues. The phosphotyrosine residues specifically recruit adaptor proteins containing SH2 (Scr Homology 2) or PTB (PhosphoTyrosine Binding) domains (Lemmon and Schlessinger, 2010). One such protein, GRB2 (Growth factor Receptor Bound protein 2), is either recruited and activated directly by the phosphotyrosine residues or via another adaptor protein, SHC (Scr Homology 2 domain Containing) (Wetzker and Böhmer, 2003). The activation of GRB2 recruits SOS (son of sevenless) a guanine exchange factor that can load GTP onto RAS (Rat Sarcoma), a small GTPase, effectively activating RAS (Marshall, 1995). GTP bound RAS leads to the activation and recruitment of RAF (Rapidly Accelerated Fibrosarcoma), a serine/threonine protein kinase, to the plasma membrane. In mammals, three RAF isoforms exist: A-RAF, B-RAF,

and C-RAF, the latter being often referred to as RAF-1 (Cseh et al., 2014). Activated RAF goes on to phosphorylate the dual-specificity protein kinase MEK (Mitogen Activated Protein Kinase Kinase). MEK has two isoforms, specifically MEK1 and MEK2. Upstream RAF activates MEK via dual-phosphorylation at serine 218/222 in MEK1 and serine 222/226 in MEK2. Activated MEK phosphorylates the master regulator of the MAPK cascade, ERK1/2. Canonical MAPK signaling can be seen in Figure 1. The two activated isoforms of ERK in turn phosphorylate and regulate substrates throughout the cell including, but not limited to, the Ribosomal S6 Kinase (RSK), Mitogen-Stress associated Kinase (MSK), and MAPK-interacting Kinase (MNK)(Cargnello and Roux, 2011), as well as transcription factors including ELK1, ETS, and STAT1/3 (Sebolt-Leopold and Herrera, 2004). Downstream effects of ERK activity modulates cellular proliferation, differentiation, migration and survival.

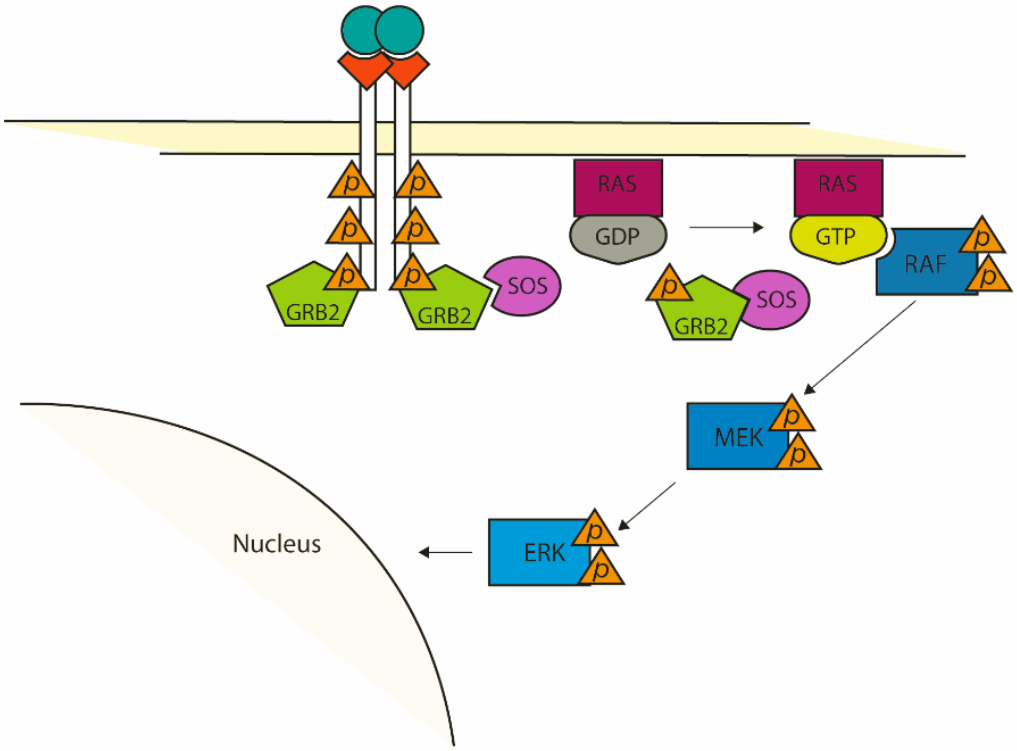

Figure 1 | *MAPK Signaling* The binding of ligands to receptor tyrosine kinases initiates dimerization and autophosphorylation of tyrosine residues. Recruitment of GRB2 and SOS leads to the activation of RAS (small GTPase). GTP bound RAS recruits RAF (MAPKKK) to the membrane, phosphorylating RAF and initiating the three tiered cytosolic cascade. Activated RAF phosphorylates MEK (MAPKK), which phosphporylates ERK (MAPK). Activated ERK has numerous downstream targets, both cytosolic and nuclear.

Due to the broad and diverse targets of MAPK signaling, mutations within the canonical pathway have numerous disease implications, specifically cancer. The most prominent oncogenic mutations associated with ERK signaling arise from the critical regulators, RAS and RAF. RAS proteins are present in all mammalian species and exist in four isoforms, specifically HRAS,

KRAS4a/4b, and NRAS. Due to the binary functionality of RAS proteins which arises from their GTPase activity, they are considered proto-oncogenes (Barbacid, 1987) and common mutations at codons 12, 13, and 61 in all RAS isoforms are found in various types of mammalian tumors (Bos, 1989). KRAS mutations, specifically at codon 12, are amongst the most common RAS mutations, as well as one of the most aggressive (Prior et al., 2012). The next node in the canonical pathway, RAF, is similarly observed in mutated states during cancer. The BRAF isoform is famous for the V600E mutation which occurs repeatedly in metastatic melanoma (Long et al., 2011). As the BRAF isoform is easily activated via phosphorylation at two sites, compared to the five sites required to activate CRAF isoforms, mutations in BRAF have been observed in approximately 7% of human cancers (Wellbrock et al., 2004) and 50% of cutaneous melanomas (Gonzalez et al., 2013). BRAF is further predominantly responsible for activating downstream MEK1/2, ultimately leading to ERK activation (Catling et al., 1994), indicating perhaps the reason for predominantly BRAF mutations associated with cancer.

Combating mutations of both RAS and RAF has ignited an era of cellular chemical warfare. RAS, a notoriously difficult target of small molecule inhibitors, has been targeted indirectly using Farnesyltransferase inhibitors which reduce RAS association to the plasma membrane (Ryan and Corcoran, 2018), targeting phosphatase SHP2 to disrupt RAS-GTP loading by SOS (Nichols et al., 2018), and inhibiting metabolic pathways which lead to increases in reactive oxidative species and cell death (Ryan and Corcoran, 2018). Direct targeting of KRAS has only most recently been brought to clinics by Amgen with their FDA approved Lumakras (Higgins-Dunn, 2021). Small molecule inhibitors targeting downstream RAF and MEK have also been used to combat mutations of RAS. Second generation RAF inhibitors that are in current use include Vemurafenib and Dabrafenib, however these inhibitors are only effective in BRAF specific mutant carcinomas. The usage of such inhibitors in cancers containing RAS mutations results in a paradoxical increase in MAPK signaling and tumor growth (Hatzivassiliou et al., 2010). For this reason, MEK inhibitors are usually favored when treating cancers expressing mutant RAS (Ryan and Corcoran, 2018).

2.2 MEK

The MAPK/ERK Kinase (MEK), also known as the Mitogen Activated Protein Kinase Kinase, is the penultimate node in canonical MAPK signaling and is duel-phosphorylated by upstream RAF at serine 218/222 (MEK1) and serine 222/226 (MEK2) (Harding and Hancock, 2008). The two isoforms of MEK are rather conserved and were once thought to be redundant. Comparison of MEK1 and MEK2 can be seen in Figure 2. The 45kDa MEK1 protein consists of an N-terminal

sequence comprised of approximately 70 amino acids which contain the ERK binding domain and nuclear export sequence, a protein kinase domain of about 290 amino acids, and a proline rich C-terminal sequence made up of nearly 30 amino acids (Roskoski, 2012). The kinase domain consists of an ATP binding domain, a catalytic core typical of all protein kinases, as well as the RAF dependent binding sites (RDS). The crucial difference between MEK1 and MEK2 stems from three specific residues that reside towards the C-terminus. MEK1 activity is negatively regulated at site T286 of MEK1 by CDK5 (Cyclin-Dependent like Kinase) phosphorylation (Rossomando et al., 1994) as well as at T292 of MEK1 by ERK phosphorylation (Brunet et al., 1994). Phosphorylation at site S298 of MEK1 by PAK1 (P21 Activated Kinase) in contrast upregulates MEK1 activity via integrin signaling (Slack-Davis et al., 2003). These three sites illuminate the difference between MEK1 and MEK2, as regulation at these sites does not occur in MEK2. Studies that further tried to dissect the difference and essentiality of MEK1 and MEK2 through *in vivo* viability experiments assessed the loss of MEK1 and MEK2. MEK1 KO mice did not survive past embryonic day 10.5, whereas MEK2 KO mice could develop normally (Giroux et al., 1999), indicating that MEK1 is indispensable for development and able to compensate for MEK2, while MEK2 is not essential (Bromberg-White et al., 2012). Deleting both MEK1/MEK2 in the epidermis during development or adulthood stunted ERK activation, resulting in hypoproliferation, apoptosis, skin barrier defects, and death (Scholl et al., 2007, p. 2). Reinstitution of either MEK1 or MEK2, or artificially stimulating ERK activity reversed the observed hypoplasia, indicating MEK1/2 are functionally redundant in the epidermis (Scholl et al., 2007).

Inhibitors of MEK have been introduced into clinics for single and combinatorial therapy (Cheng and Tian, 2017). The distinct structure and narrow substrate specificities make MEK a therapeutically interesting target, specifically in regards to the essentiality of MEK and MAPK in the progression through the G1 phase of the cell cycle (Zhao and Adjei, 2014). Conceptually, hindering MAPK signal propagation should arrest uncontrollably proliferating cells. Many MEK inhibitors are innovative in their uncompetitive ATP binding mechanism, targeting instead a pocket adjacent to the ATP binding site. Using this pocket instead of the ATP binding site eliminates inadvertent inhibition of other kinases containing the conserved ATP binding motif (Ohren et al., 2004). Other MEK inhibitors are allosteric in their mode of action, often constraining the movement of the activation loop, decreasing phosphorylation from upstream activators, i.e. RAF (Liu and Gray, 2006). Currently, four MEK inhibitors are FDA approved, these being trametinib, selumetinib, cobimetinib and binimetinib (Han et al., 2021) Indications for the different MEK inhibitors include melanoma, non-small cell lung cancer, thyroid cancer, and neurofibroma (Han et al., 2021).

The first FDA approved MEK inhibitor, trametinib, was developed by Novartis and released in 2013 (Reddy et al., 2017). Zooming in on trametinib as an example of a MEK inhibitor: it is an orally available, small molecule, with both allosteric and noncompetitive ATP inhibitor properties. Trametinib has a terminal half-life of 5.3 days and a low likelihood of drug-drug interactions based on its inability to inhibit most critical cytochrome enzymes in the liver

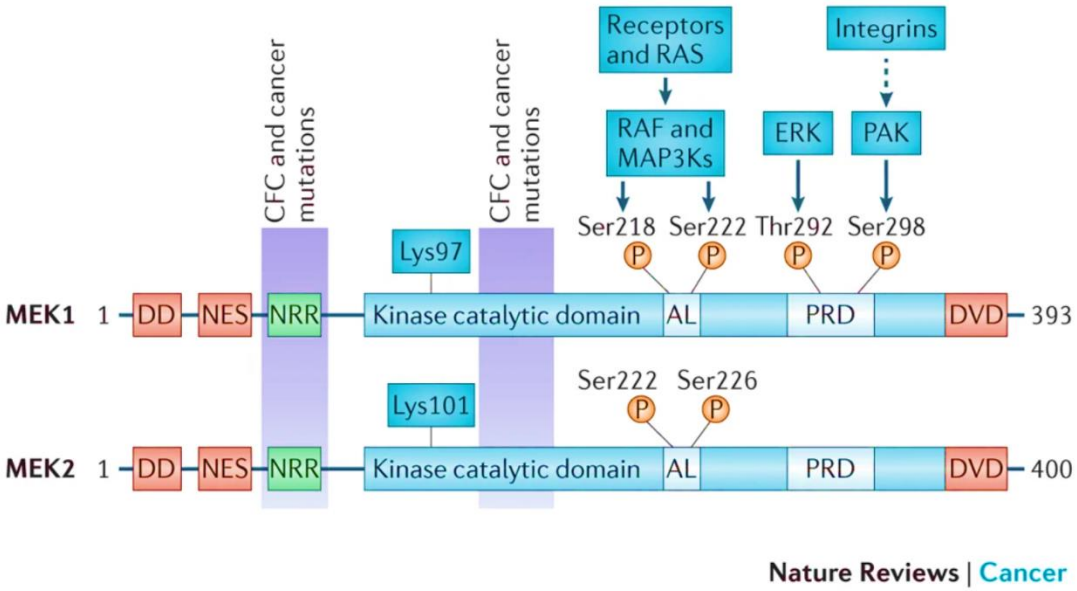

Figure 2 | *Structure of MEK1 & MEK2* Linear schemes depicting domains present in MEK1 and MEK2. The ERK docking domain (DD), nuclear export sequence (NES) and negative regulatory region (NRR) is conserved between the two MEK variants. Mutations in NRR have been observed in cancer and CFC (cardo-facio-cutaneous) syndrome. The kinase domain contains an activation loop (AL) and a proline rich domain (PRD). The AL contains the RAF dependent activation sites, serine 218/222 and serine 222/226 for MEK1 and MEK2, respectively. Critical regulatory sites existing in MEK1 that are absent in MEK2 include threonine 292, the site of ERK feedback regulation, and serine 298, the site of PAK activation following integrin signaling. The domain of versatile docking is present in both forms of MEK. *From* (Caunt et al., 2015)

(Lugowska et al., 2015). Trametinib has been approved for combinatorial therapy with BRAF inhibitors such as dabrafenib to treat metastatic melanoma (Hoffner and Benchich, 2018). The quality of life associated with trametinib treatment compared to standard chemotherapy treatment of advanced melanoma was investigated in a randomized phase III study. Results showed that trametinib treatment indicates less functional impairment, smaller declines in health status, and decreased exacerbation of symptoms compared to chemotherapy (Schadendorf et al., 2014).

2.3 MEK1 Mutants

Based on the regulatory sites present only in MEK1 and the essentiality of MEK1 in embryonic development, it proves critical to better understand MEK1 activity as it relates to MAPK signaling and cell biology at large. Looking at the distribution of MEK1 throughout the cell in Figure 3, it is difficult to imagine that the sole purpose of MEK1 is to activate downstream ERK.

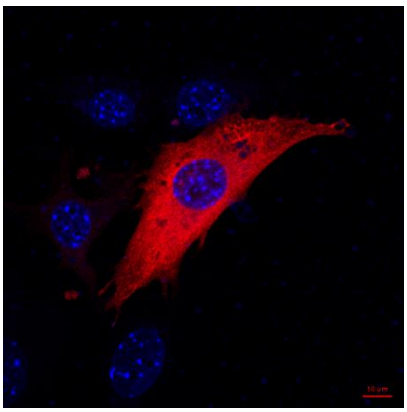

Figure 3 | *MEK1 Localization* Confocal image of MEK1 distribution in a mouse embryonic fibroblast cell. MEK1 red | DAPI blue

To better understand the role, and perhaps moonlighting functions of MEK1, specific point mutations can be induced to create snapshots of MEK1 in different states. For example, the serine 218/222 RDS can be mutated to alanine (S218/222A), essentially blocking phosphorylation, and therefore stopping activation by upstream RAF. Similarly, the serine 218/222 residues can be mutated to aspartic acid (S218/222D) to mimic RAF phosphorylation, providing a constitutively active MEK1 model. The aforementioned ERK dependent deregulation of MEK1

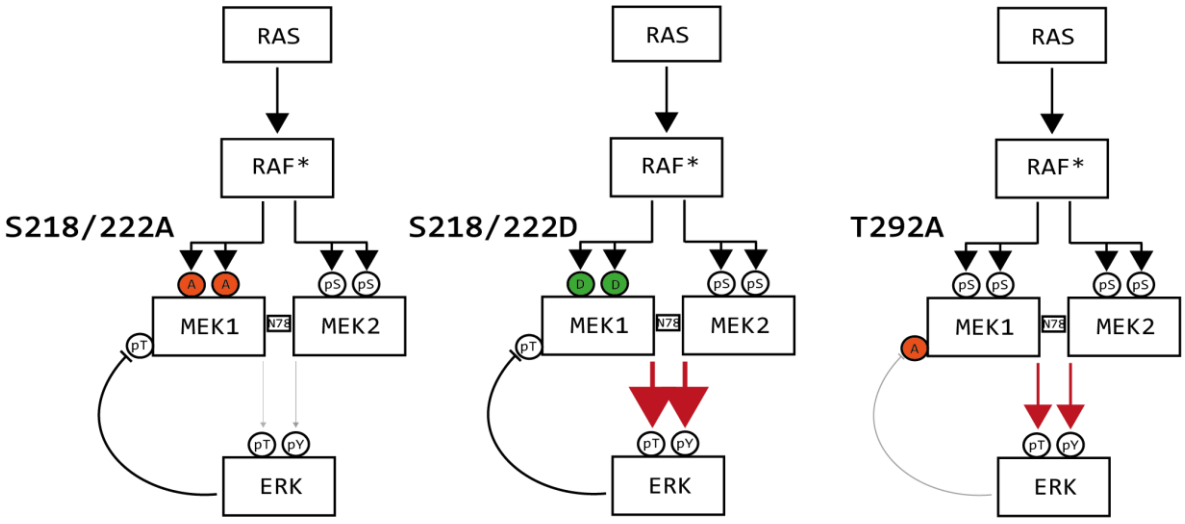

Figure 4a | *Mutations of MEK1* Alanine and aspartic acid substitutions at RDS mimic constitutively inactive/active forms of MEK1, effects on downstream ERK activation can be observed. Alanine substitution for threonine 292 stops ERK feedback inhibition of MEK1.

activity can also be assessed using alanine and aspartic acid substitutions at T292 to mimic constitutively phosphorylated and dephosphorylated states, specifically T292A and T292D mutations. Research has shown the strength of MEK phosphorylation on downstream ERK is enhanced through the formation of MEK1/MEK2 dimers (Catalanotti et al., 2009). It is further

known that mutations at the asparagine 78 residue destabilize the MEK1/MEK2 dimer. Thus, substitution of glycine for asparagine (N78G) effectively reduces the dimerization ability of MEK1 and MEK2, stunting downstream ERK activation.

While disease inducing mutations associated with ERK signaling occur predominantly in upstream RAF and RAS, mutations of MEK1 have also been observed in various states of disease. Constitutive activation of MEK1, achieved experimentally via the S218/222D mutation, has been shown to induce melorheostotic bone disease in mice, mirroring clinical data of MEK1 mutations

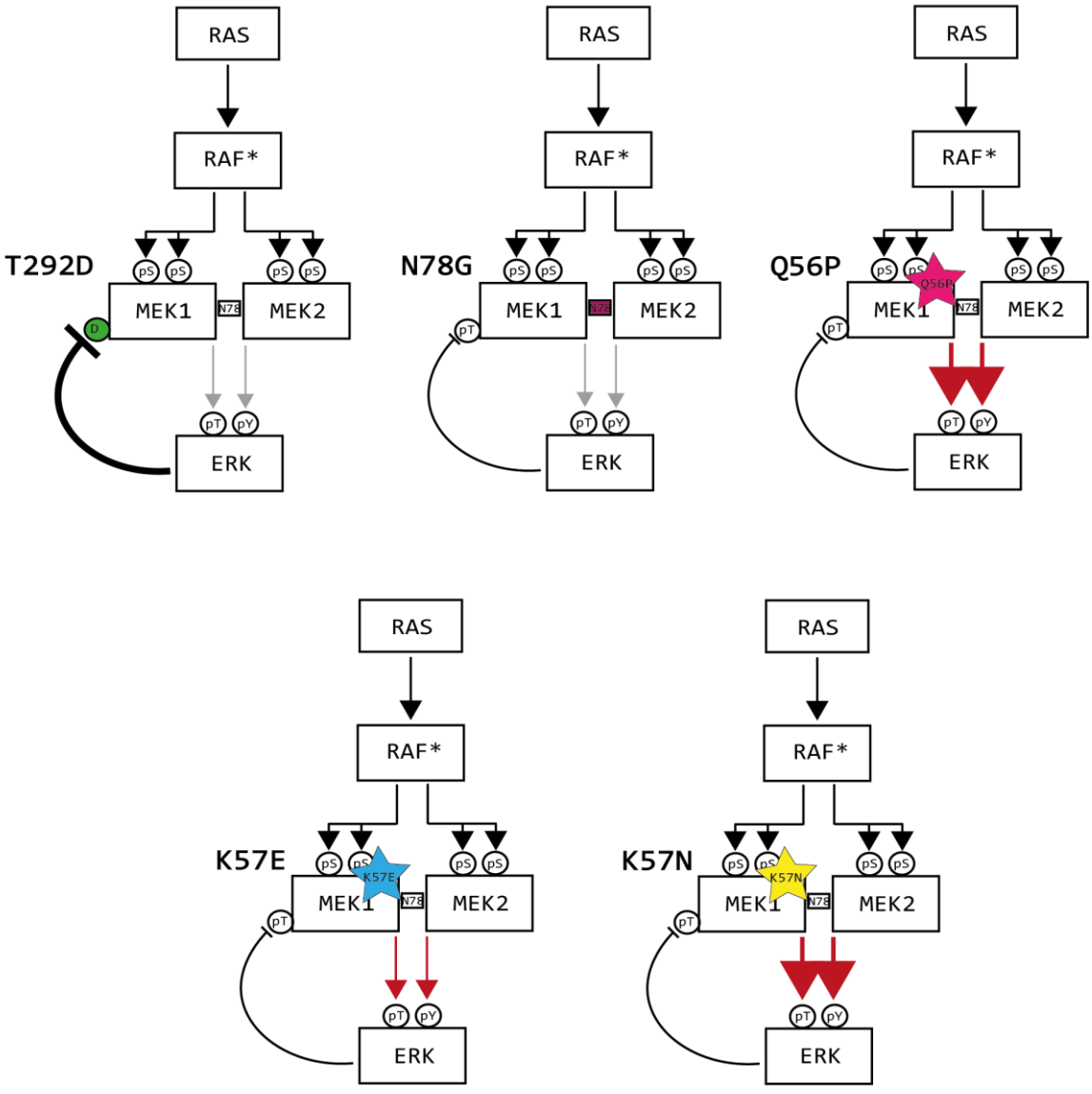

Figure 4b | *Mutations of MEK1* Aspartic acid substitution for threonine 292 mimics continuous ERK feedback inhibition of MEK1. Disruption of MEK1-MEK2 dimer is achieved via the N78G mutation. Various mutations within the kinetic domain indicated in disease include Q56P, K57E and K57N. The expected effects of the various mutations on MAPK signaling can be seen in each individual diagram.

that induce constitutive MEK1 activity (Fowlkes et al., 2020). These mutations occur predominantly in the negative regulatory domain of MEK1, specifically mutations in glutamine at residue 56 for proline (Q56P) and lysine at residue 57 for asparagine or glutamic acid (K57N / K57E) (Kang et al., 2018). These mutations are also known to occur in various cancer indications in conjunction with other classical oncogenic MAPK mutations such as BRAF V600E in melanoma. The mutations lead to a gain of function in MEK1 activity by inhibiting the negative regulation of MEK1, resulting in increased downstream ERK phosphorylation and activation. The mutations have been observed in various cancer types, including lung (Marks et al., 2008), skin, colorectal (Murugan et al., 2009), and hairy cell leukemia (Waterfall et al., 2014). Mutations of MEK1 have also been shown to develop in melanoma as a mode of resistance to BRAF inhibitors such as vemurafenib (Trunzer et al., 2013). For this reason, investigation of MEK1 mutants Q56P, K57E, and K57N in an experimental setting will provide unique insight into the aberrant activity of MEK1 observed in disease states.

2.4 Proximity Dependent Labeling

Untangling the protein-protein interactions (PPIs) that drive cellular biology is essential to better understand the nature of cell signaling as it relates to life, proliferation, and senescence. Determination of protein interactions is often achieved through immunoprecipitation techniques which make use of an antibody's affinity to an antigen (i.e. the protein of interest) (Kaboord and Perr, 2008). Harnessing this affinity allows the antigen, as well as the proteins bound to the antigen, to be isolated and analyzed. While this technique enables the determination of stable interaction partners, it fails to capture weaker, more transient interactions which are easily lost through cell lysis and various wash steps (Qin et al., 2021). Due to the complexity of signal regulation and propagation, it is essential to understand both stable, as well as nondescript, PPIs.

Proximity dependent labeling (PDL) involves engineering bait proteins tagged with specific enzymes that are able to label proximal proteins within nanometer distance. Examples of such enzymes include peroxidases, as seen in APEX systems (Lam et al., 2015), and biotin ligases, as seen in BioID (Roux et al., 2012) and TurboID (Branon et al., 2018). All systems require the addition of biotin as a substrate, which is then attached to proximal proteins with accessible Lysine or Tyrosine residues via enzymatic activity. Biotin labeled proteins can then easily be extracted from the system using the natural affinity of biotin to streptavidin (Weber et al., 1989). In the APEX system, biotin phenol is added to the cell culture media prior to the experiment. The addition of H_2O_2 initiates the biotinylation which shortly after requires quenching with buffers

containing peroxidase inhibitors and competitive substrates (Lobingier et al., 2017). The application of APEX, however, is limited, specifically in regards to cell signaling investigation, due to the inherent toxicity of H_2O_2 (Qin et al., 2021). The promiscuous biotin ligases used in BioID and TurboID provide an alternative to the peroxidase system. Originating from an

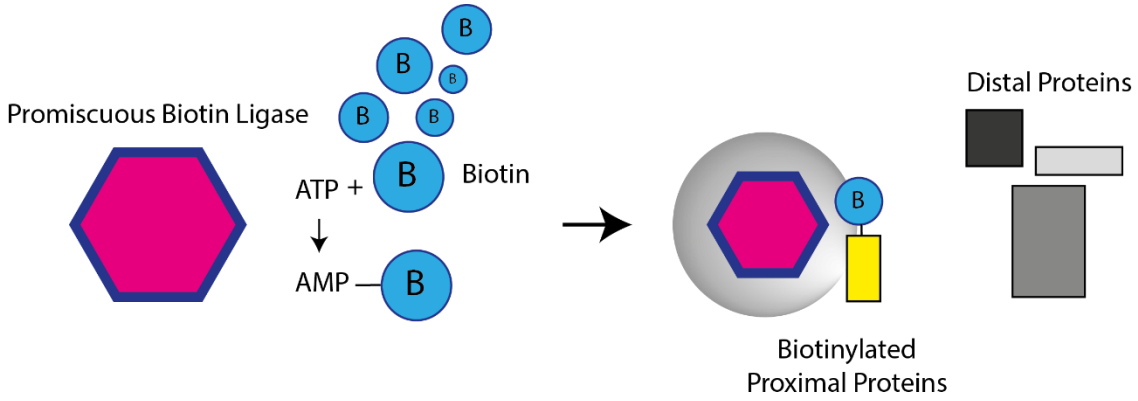

Figure 5 | *TurboID Scheme* By attaching the promiscuous biotin ligase to a protein of interest, proximal proteins can be labeled by adding biotin to the system. The ligase converts endogenous ATP to Biotin-AMP, a reactive intermediate that covalently labels proximal proteins.

Escherichia coli biotin protein ligase (Roux et al., 2012), BioID allows for the labeling of proximal proteins without the addition of harsh compounds which likely influence cellular signaling networks. Only the addition of biotin is required to initiate biotinylation of proximal proteins. Despite the simplicity of the BioID system, initial experiments required long biotin exposure times of 18 hours (Branon et al., 2018). While this still allowed for time-lapse-like understanding of PPIs, it failed to provide snapshots of interactions. This led to the development of TurboID, which effectively labels proximal proteins in minutes rather than hours. TurboID is 35kD and can be appended to any protein of interest to label proximal proteins over the course of a 10 minute protocol, providing a snapshot of protein activity (Cho et al., 2020). TurboID however has a relatively high affinity for biotin and therefore requires stringent controls to parse false positives from resulting data. MiniTurbo is smaller (28kD) and has a two fold lower biotin affinity compared to TurboID, providing better temporal resolution and reduced labeling resulting from endogenous biotin (Cho et al., 2020).

2.5 Metabolism

For cells to function, sufficient energy is required. The bulk of this energy stems from Adenosine Triphosphate (ATP). At a structural level, ATP is a prime proprietor for energy storage based on its highly exergonic profile post hydrolysis, in conjunction with its kinetic stability at a neutral pH. Thus the cleavage of the phosphoanhydride bond, and the resulting release in energy, is achieved only in the presence of enzymes, making ATP a critical cofactor in diverse cellular processes (Nelson, 2017). In order to provide cellular mechanisms with sufficient energy, metabolic pathways exist to import and convert extracellular nutrients into ATP. Six main pathways of cellular metabolism are regulated in order to effectively sustain a cell's energy needs. These pathways include glycolysis, the tricarboxylic acid (TCA) cycle, fatty acid oxidation (FAO), fatty acid synthesis (FAS), amino acid metabolism, and the pentose phosphate pathway (PPP).

The "sweet breakdown" known as glycolysis was the first metabolic pathway to be defined and is perhaps the best understood (Nelson, 2017). Glycolysis involves the conversion of one glucose molecule into two pyruvate molecules. Taking place in the cytoplasm, it is one of the most ancient energy production pathways, occurring before oxygen was readily available in the atmosphere to support life. Energetically, glycolysis can be seen as unfavorable, as only two molecules of ATP are produced per glucose molecule. This lack of energy output is compensated by the production of pyruvate, which provides the carbon required for many downstream biosynthetic reactions as well as chemical potential energy that can be extracted downstream by oxidative reactions in the TCA cycle (Nelson, 2017). In addition to pyruvate and ATP, glycolysis also produces two molecules of the reduced form of Nicotinamide Adenine Dinucleotide (NADH) per molecule of glucose, which acts as a cofactor for many enzymes.

The TCA cycle, also known as the citric acid cycle or the Krebs cycle, occurs within the mitochondria matrix (Berg et al., 2002). The cycle comprises numerous oxidative reactions, beginning with the condensation of acetyl coenzyme A (acetyl-CoA) with oxaloacetate into citrate. During each cycle, three NADH molecules and one $FADH_2$ molecule are generated, as well as one molecule of GTP or ATP. NADH and $FADH_2$ are critical cofactors in the electron transport chain (ETC), aiding in oxidative phosphorylation (OXPHOS) which is the main production center of ATP, and thus the main energy source for quiescent and non-proliferating cells.

Fatty Acid Oxidation involves the conversion of fatty acids into acetyl-CoA which can then be fed into the TCA cycle. Short fatty acids with less than 12 carbons can enter the matrix without the help of transporters (Nelson, 2017). Longer fatty acids must be "activated" in the cytosol and transported into the mitochondria via the carnitine shuttle. Once short and long fatty acids make

their way into the matrix, they can be converted to acetyl-CoA and used to generate essential cofactors for the ETC, ultimately leading to ATP production.

As a counterpart to FAO, Fatty Acid Synthesis occurs when ample levels of carbohydrates are present, relieving the need to convert fatty acids into energy. Superfluous carbohydrates are converted and stored as fatty acids in the cytosol while simultaneously inhibiting carnitine shuttling via the premier FAS enzyme, malonyl-CoA (Nelson, 2017).

Amino acids, aside from being the building blocks of proteins, can also be utilized as substrates for ATP production. Amino acids are categorized often as ketogenic or glucogenic, according to their major degradative end product (Nelson, 2017). In general, ketogenic amino acids degrade to acetyl-CoA, either entering the TCA cycle or developing into ketone bodies. Glucogenic amino acids are shuttled into the TCA cycle, often through their degradation to glutamate, which can then undergo glutaminolysis. Research has shown promising implications of targeting glutaminolytic enzymes as an anti-cancer therapy (Jin et al., 2016).

The pentose phosphate pathway occurs in the cytosol as an offshoot of the first step in glycolysis. Instead of producing ATP and pyruvate, the PPP yields ribose 5-phopshate and NADPH which aid in nucleic acid synthesis and fatty acid/sterol/nucleotide synthesis respectively(Ge et al., 2020) .

The chorus of metabolic pathways provide systematic regulation of a cell's energy needs. In states of disease, specifically cancer, these pathways are often compromised. As such, it is essential to deepen our understanding of the coordination between metabolism and other essential signaling pathways.

2.6 The Warburg Effect and cancer metabolism

The interplay between metabolism and cancer has been thematically relevant for nearly a century since the critical observations of Otto Warburg, which defined a glycolytic shift associated with carcinoma cells (Warburg, 1925). In low oxygen conditions, cells have been observed to shift to a glycolysis centered metabolism known as anaerobic glycolysis. In a tumor environment, cells often become overcrowded, reducing the oxygen availability as blood vessels fail to sustain the rapid tissue growth. Warburg interestingly found that this glycolytic shift occurred in carcinoma cells that were supplied with sufficient amounts of oxygen, known as aerobic glycolysis (Warburg, 1925). While Warburg received the Nobel Prize for Medicine in 1931 for his discovery, it is clear today that the strict dichotomy of cancer metabolism is more complicated and nuanced than once believed.

In general, glycolysis and oxidative phosphorylation (OXPHOS) are inversely correlated with one another, and the balance between these two pivotal energy pathways is essential to provide the optimal metabolism for various cell states (Zheng, 2012). Warburg's conjecture that compromised respiration not only characterizes, but causes cancer (Warburg, 1956) is false, as mitochondrial OXPHOS is not impaired in carcinomas and oxidative metabolism is still observed (Kroemer and Pouyssegur, 2008). This being said, the increase in glucose uptake, associated with a glycolytic shift as defined by Warburg, is still effectively utilized in clinics coupled with PET (Positron Emission Tomography) imaging and radiopharmaceutical glucose analogs (Fludeoxyglucose) to localize and monitor tumor growth (Mankoff et al., 2007). Drug discovery endeavors focused on developing effective combinatorial therapies have, amongst other techniques, turned to metabolic modulation. Using glycolytic inhibitors in metastatic melanoma models in conjunction with vemurafenib resulted in increased efficacy (Abildgaard et al., 2021). Metabolism proves to be a unique avenue for novel, innovative technologies to better monitor and combat aberrant cell proliferation. Thus it is important to enrich the understanding of critical nuances in cancer metabolism.

Metabolic aspects of cancer include metabolic reprogramming and elevated production of so called oncometabolites. Reprogramming results most often from aberrant signaling of oncoproteins, leading to an enhancement of conventional metabolic pathways (DeBerardinis and Chandel, 2016). As an example, the increased activation of the PI3K/Akt pathway, associated with numerous maladies, leads to increased glucose uptake and glycolysis (Buzzai et al., 2005). Exacerbation of PI3K/Akt signaling also leads to increased activity of downstream mTORC1, which is best known for enhancing protein synthesis, as well as promoting mitochondrial metabolism (Ward and Thompson, 2012). Oxaloacetate, a TCA cycle intermediate, can be transaminated to form aspartate, a critical precursor for de novo asparagine production. This ability of cancer cells explains treatment failures associated with depleting asparagine levels in blood plasma in adults via L-asparaginase treatment (Clarkson et al., 1970).

As a further example of metabolic reprogramming, transcription factor MYC, often overexpressed through aberrant MAPK signaling, has been shown to stimulate transcription of mitochondrial genes located in the nucleus and promote mitochondrial biogenesis (Li et al., 2005). MYC induces the expression of glutaminase, which is responsible for the conversion of glutamine to glutamate, a critical step in glutamine metabolism (Ward and Thompson, 2012). Further, it has been shown that oncogenic expression of MYC is associated with an increased catabolism of glutamine via heightened glutaminolysis (Wise et al., 2008), leading such cells to have an "addiction" to glutamine as a bioenergetic substrate.

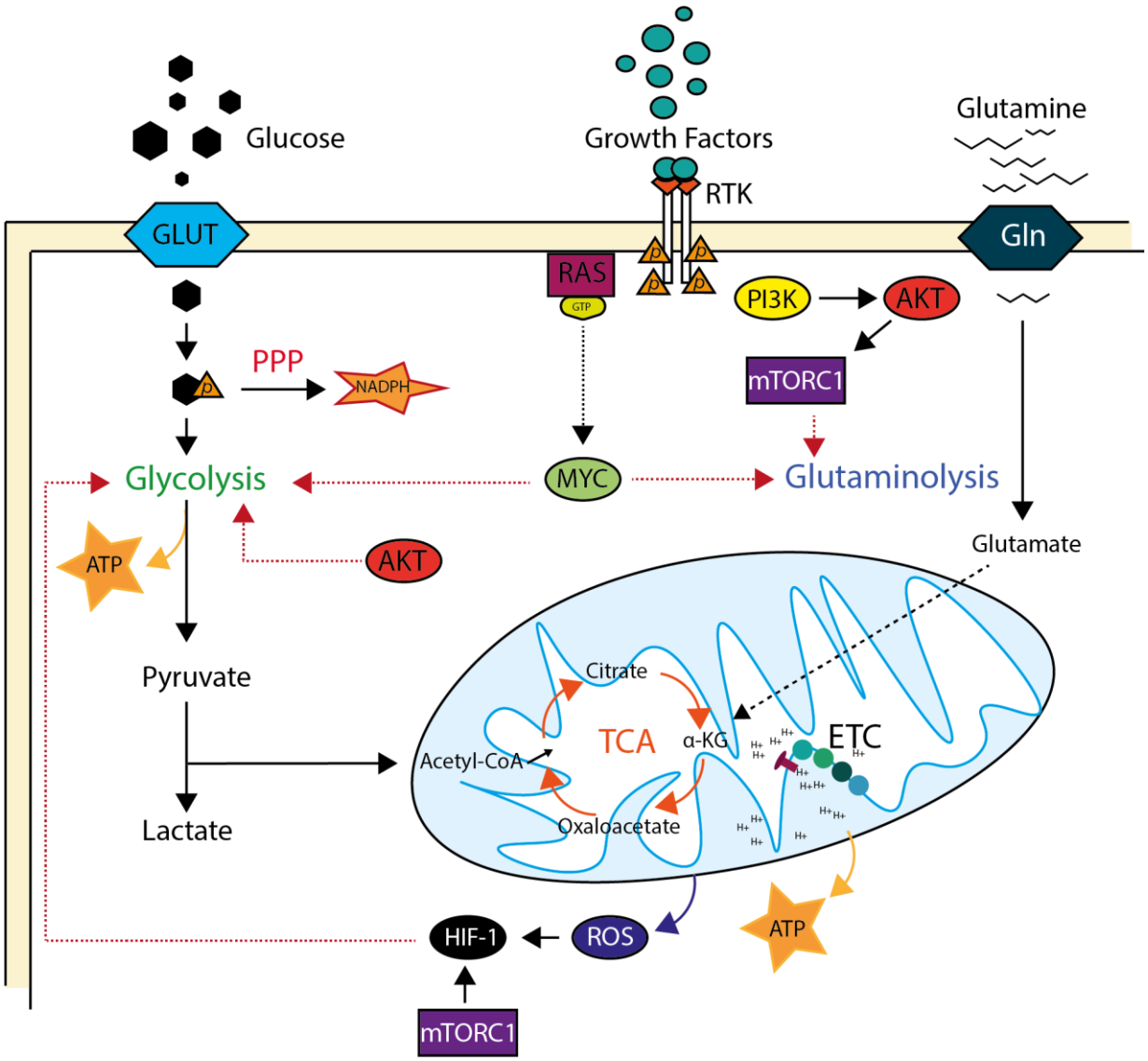

Figure 6 | ***Selection of Metabolic Pathways and Various Disease Associated Modulations*** Glucose and glutamine enter cells through glucose transporters (GLUT) and glutamine transporters (Gln), respectively, and are eventually fed into the TCA cycle, or turned to lactate (only glucose). Glucose 6 Phosphate, the first step of glycolysis, can enter the pentose phosphate pathway, increasing NADPH production. Overexpression of MYC from upstream MAPK signaling increases glutaminolysis and modulates glycolysis, promoting anabolism. PI3K/AKT activates mTORC1 inducing anabolic growth and activated AKT increases glucose uptake. Active mTORC1 increases transcription of HIF-1, which is stabilized by ROS, ultimately promoting glycolysis.

The list of currently confirmed oncometabolites remains rather short, consisting of fumarate, succinate, and D 2-hydroxyglutarate (D 2-HG) (Yang et al., 2013). By definition, oncometabolites not only robustly accumulate in certain cancers, acting as a biomarker, but also have been shown to directly contribute to cellular transformation (Collins et al., 2017). Fumarate and succinate are intermediates of the TCA cycle and have been shown to be massively overproduced in various cancer types due to loss-of-function mutations in fumarase and succinate dehydrogenase (DeBerardinis and Chandel, 2016). Aside from metabolite build up, it has also

been indicated that fumarate and succinate regulate hypoxia-inducible genes via epigenetic regulation of TET enzymes (Laukka et al., 2016). To a similar extent, D 2-HG is the reduced from of TCA cycle intermediate α ketoglutarate and is generated through mutations in isocitrate dehydrogenase (DeBerardinis and Chandel, 2016). In an unmutated state, D 2-HG levels are scarce. For this reason, D 2-HG is also a biomarker for monitoring disease states. Increases in D 2-HG further have been shown to play a role in histone methylation, ultimately regulating the expression of ZEB1, a master regulator of epithelial-mesenchymal transition. As such, D 2-HG has been indicated as a driver for metastasis in colorectal cancer (Colvin et al., 2016)

2.7 Mitochondria and their disease implications

Touted in biology classrooms around the world as the "powerhouse" of the cell, the mitochondria facilitate the majority of ATP production and are a critical organelle in respect to metabolism. The origin of mitochondria in eukaryotic cells is debated. One hypothesis indicates mitochondria arose from prokaryotes capable of oxidative respiration, forming an endosymbiotic relationship with eukaryotic cells. This hypothesis would explain the unique mitochondrial genome, which consists of 37 genes encoding 13 proteins, 2 ribosomal RNAs, and 22 tRNAs (Gustafsson et al., 2016). To function, the mitochondria require magnitudes of proteins more than the 13 proteins transcribed from mitochondrial DNA (mtDNA) (Sickmann et al., 2003). This indicates the endosymbiotic relationship between mitochondria and the host eukaryotic cell has evolved significantly, relocating the genes for a majority of mitochondrial proteins to the nuclear genome. As an example, the electron transport chain requires nearly 90 different proteins for OXPHOS. 13 of these proteins arise from the mitochondria genome and the rest are nuclear in origin. It has been shown however, that the small subset of mitochondrial proteins partaking in OXPHOS are essential, as stopping mtDNA transcription disrupts OXPHOS (Larsson et al., 1998).

The high output of ATP resulting from the oxidative reactions occurring during OXPHOS leads to the production of reactive oxidative species (ROS) within the cell. Superoxide radicals are produced in the mitochondria and are then converted to hydrogen peroxide via superoxide dismutase (SOD) (Loschen et al., 1974). ROS production leads to redox signaling, as well as mitochondrial disfunction, apoptosis, and disease (Murphy, 2009). While a spectrum of malignancies exist associated with abnormalities in the mitochondria, explained acutely by the United Mitochondrial Disease Foundation ("Mitochondrial Disease | UMDF," n.d.), mitochondrial production of ATP and ROS have critical implications in cancer. As discussed in previous sections, the balance of metabolic pathways for ATP production has been shown to be ever more

important in understanding metabolic aspects essential in oncology. Since mitochondrial ATP production is inherently coupled with ROS generation, modulations of mitochondrial ROS and redox signaling could provide new opportunities to target aberrant cell growth. Complexes I, II, and III in the ETC have the ability to produce ROS within the mitochondria matrix. Ubiquinone delivers electrons generated in Complex I and II to Complex III. As two electrons must be loaded to the ubiquinone, semiubiquinone intermediates at times arise. The semiubiquinone binding site of Complex III is located near the intermembrane space. The strong electrical gradient of the inner mitochondria membrane (IMM), -180mV, often accelerates superoxide production in the intermembrane space via semiubiquinone (Sabharwal and Schumacker, 2014). ROS produced in the intermembrane space has been shown to be hypoxia dependent, increasing in hypoxic states (Guzy et al., 2005).

The production of ROS within the mitochondria matrix has the propensity to damage mitochondrial protein machinery as well as induce mutations in the mitochondrial genome. ROS exiting the mitochondria induces redox-dependent inhibition of prolyl hydroxylases (PHDs) which leads to hypoxia induced factor (HIF) activation (Sabharwal and Schumacker, 2014). HIF

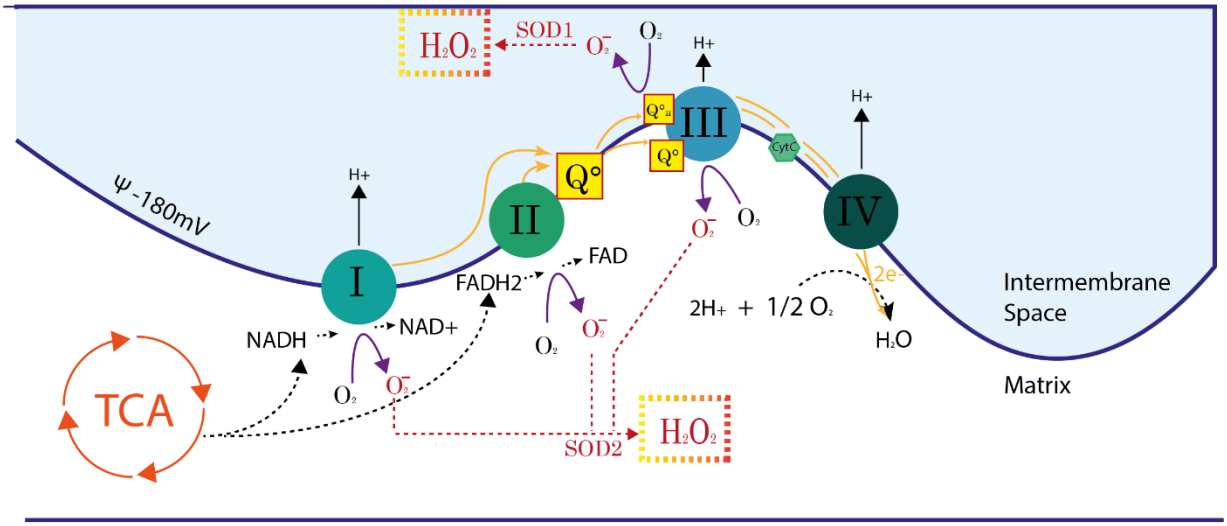

Figure 7 | *Superoxide Production in the ETC* Products of the TCA cycle provide substrates for Complex I & II of the ETC. Complex I & II transfer electrons to ubiquinone (Q°) which relays pairs of electrons to complex III where electrons are shuttled via cytochrome c (CytC) to complex IV. Free oxygen can capture electrons being transferred through the chain of redox reactions, generating superoxide (O_2) which are converted to hydrogen peroxide by superoxide dismutase (SOD). The production of ROS in the intermembrane space occurs when singly loaded ubiquinone (semiubiquinone) binds to complex III. The combination of the outward location of the semiubiquinone binding site and the strong electron field generated by the inner membrane potential (-180mV) accelerates superoxide production in the intermembrane space. *Scheme from* (Sabharwal and Schumacker, 2014)

activation has the ability to induce numerous genes essential for cancer biology, leading to angiogenesis, cell survival/proliferation, glucose metabolism, and apoptosis(Semenza, 2003). It

has been shown that oncoproteins promote tumor generation via ROS production. In KRAS mutants, a fluorescent redox sensor showed increased ROS production in the mitochondria matrix, specifically linked to Complex III activity (Weinberg et al., 2010). Further, the importance of ROS production in disease progression was shown in a KRAS driven mouse model for lung cancer. Disrupting ETC and mitochondria function by blocking mitochondrial transcription factor TFAM in KRAS mutant mice reduced tumorigenesis (Weinberg et al., 2010).

Apart from fluctuations in ROS production, further perturbations of mitochondria biology have shown to be affected by various proto-oncogenes. Overexpression of HIPK in Drosophila has been shown to induce hyperpolarization of the mitochondria membrane, leading to tumor like growth (Wong et al., 2020). In BRAF 600E melanoma, treatment with vemurafenib and trametinib have been shown to severely reduce glycolysis, leading to a survival dependent increase in OXPHOS post-treatment (Abildgaard and Guldberg, 2015). As such, it was postulated that inhibiting inner mitochondria membrane function, the site of OXPHOS, as well as outer mitochondria membrane function, a major site of anti-apoptotic BCL-2 protein function, could be a fruitful additional therapy to combat resistances arising from vemurafenib and trametinib (Serasinghe et al., 2018). The authors of the study concluded the inhibition of both inner and outer mitochondria membranes would increase the efficacy of pro-apoptotic effects of MAPK inhibitors, helping to eradicate cancer cells, prevent resistance, and support long term remission (Serasinghe et al., 2018). The interconnectivity of mitochondria functionality with other critical signaling pathways in states of health and disease provides an exciting landscape for novel cancer treatments. As such, it is essential to further dissect the role of canonical pathways, specifically the RAS/ERK signaling pathway, in the metabolic reprogramming associated with disease states.

3. Materials

Flow Cytometry Staining

Stain	Concentration	Fluorochrome	Producer	Cat. No.
TMRE	200 nM	PE-A	ThermoFischer	T669
MitoTracker green	50 nM	FITC-A	ThermoFischer	M7514
eBioscience Fixable viability dye	1µL / 10 x 10^6 Cells	CY 7	Invitrogen	65-0865-14
CellROX Deep Red	5µM	APCA	Invitrogen	C10422

Primary Antibodies

Antigen	Dilution	Diluent	Species	Producer	Cat. No.
Calreticulin	1:1000	3% BSA/TBST	Rabbit	CST	12238
pERK	1:1000	3% BSA/TBST	Rabbit	CST	9101
tERK	1:1000	3% BSA/TBST	Rabbit	CST	9102
GAPDH	1:1000	3% BSA/TBST	Rabbit	Millipore	ABS16
Golgin	1:1000	3% BSA/TBST	Rabbit	CST	13192
HIF1α	1:1000	3% BSA/TBST	Rabbit	Upstate	07-628
HK2	1:1000	3% BSA/TBST	Rabbit	CST	2106
Lamin	1:1000	3% BSA/TBST	Mouse	CST	4777
LAMP 1	1:1000	3% BSA/TBST	Mouse	abcam	Ab25630
tLDHA	1:1000	3% BSA/TBST	Rabbit	CST	2012
pLDHA	1:1000	3% BSA/TBST	Rabbit	CST	8176
MEK1	1:1000	3% BSA/TBST	Mouse	CST	2352
MEK2	1:1000	3% BSA/TBST	Rabbit	CST	9125

pMEK1 T292	1:1000	3% BSA/TBST	Rabbit	CST	26975
pMEK1 RDS	1:1000	3% BSA/TBST	Rabbit	CST	9121
RAB7	1:1000	3% BSA/TBST	Rabbit	CST	9367
Tubulin	1:1000	3% BSA/TBST	Rabbit	CST	2125
VDAC	1:1000	3% BSA/TBST	Rabbit	CST	4661

Secondary Antibodies

Antigen	**Dilution**	**Diluent**	**Producer**	**Cat. No.**
α Mouse	1:5000	5% Milk TBST	GE Healthcare	NA 931V
α Rabbit	1:5000	5% Milk TBST	GE Healthcare	NA 934V

Western Blot gel preparation

10% SDS PAGE	Running GEL (20ml)		Stacking GEL (15ml)	
ddH20	7.9ml	15.5ml	8.4ml	16.8ml
30% Acrylamide mix	6.7ml	13.4ml	2.5ml	5.0ml
1.5M Tris (pH 8.8)	5ml	10ml	----------	----------
0.5M Tris (pH 6.8)	----------	----------	3.7ml	7.4ml
10% SDS	200ul	400ul	150ml	300ml
10% APS	200ul	400ul	150ul	300ul
TEMED	20ul	40ul	15ul	30ul

Mitochondria Isolation Buffers

- ¶ OptiPrep™ (60% with iodixanol)
- ¶ Homogenization medium: 0.25M sucrose, 1 mM EDTA, 20mM Hepes-NaHO @ pH7.4.
- ¶ Diluent: 0.25M sucrose, 6mM EDTA, 120mM Hepes-NaOH @ pH 7.4
- ¶ Working solution of 50% iodixanol: 5 OptiPrep™ : 1 Diluent

Abcam Mitochondria Isolation Kit (ab110170)

Mitochondrial isolation protocol summary:
- suspend cells in reagent A and incubate for 10 min
- homogenize using dounce homogenizer
- spin at 1,000 g for 10 min and retain supernatant, repeat
- spin at 12,000 g for 15 min and retain pellet
- resuspend pellet in reagent C and analyze or freeze

qRT-PCR Primers

Atp5h_Fwd	AATGAGACCTTCCACGCCAG
Atp5h_Rev	GCACAGGAATCTTCAGGGCA
Hk2_Fwd	TGATCGCCTGCTTATTCACGG
Hk2_Rev	AACCGCCTAGAAATCTCCAGA
Suclg1_Fwd	CACGGGTCTTACACAGCCTC
Suclg1_Rev	ACTCCAAAGCCTGCTGACTG
Pdhx_Fwd	CTGTCGAAGAAAGCACGGGA
Pdhx_Rev	AGCGAACTCATCGATGCCAA
Cox5b_Fwd	TAGCAGCACAGAAGGGACTG
Cox5b_Rev	CTTGTTGCTGATGGACGGGA
LDHA_Fwd	GCG GCT ACA CGT ACA CGG
LDHA_Rev	ATCCATCATCTCGCCCTTGAG
Irs1_Fwd	CGATGGCTTCTCAGACGTG
Irs1_Rev	CAGCCCGCTTGTTGATGTTG
Cs_Fwd	GCCTGTGCCGGTTTGTCTAC
Cs_Rev	CAAGGACGAGGCAGGATGAG
Ndufb5_Fwd	CGAAGACTGTCGCTCCTGT
Ndufb5_Rev	GGGATCCCAGTCAACATAAGGT
Slc25a22 _Fwd	CCCCATCGACCTGGCTAAGA
Slc25a22_Rev	TGCTGCTCCCCTATACATGCC
Slc2a1(Glut1)_Fwd	CAGTTCGGCTATAACACTGGTG
Slc2a1(Glut1)_Rev	GCCCCCGACAGAGAAGAT G
Pdha1_Fwd	TCACTGCGTTTTGGGCGT
Pdha1_Rev	TTACGGGAAGCAACCAGCAC
Eno3_Fwd	GCAATCCCGACCTCGTACTC
Eno3_Rev	TTGAAAGAGCTGGCTCCCAC
HIF1A_Fwd	GGGTACAAGAAACCACCCAT
HIF1A_Rev	GAGGCTGTGTCGACTGAGAA
Sdha_Fwd	TGCGGCTTTCACTTCTCTGT
Sdha_Rev	GAAAGGCCAAATGCAGCTCG

4. Methods

4.1 Cell culture

Human Embryonic Kidney (HEK) cells and Mouse Embryonic Fibroblasts (MEFs) were cultured in mycoplasma free conditions in normal medium (DMEM supplemented with 10% FCS and Penicillin / Streptomycin). Adherent cells were split using warm Trypsin. For western blot analysis, cells were grown in 10cm petri dishes, for q-RT-PCR in 6 well plates, for flow cytometry in 3cm petri dishes, for mitochondria isolations in 15cm petri dishes. Experiments were conducted when cells reached 80% confluency. MEK constructs were expressed in a wild type (WT) background in HEK293T cells and in a MEK1 KO background in MEF cells. All constructs can be expressed via a Doxycycline (DOX) inducible system and are tagged with TurboID and a V5 tag. DOX was added for 24 hours with concentration 0.5µg/ml in HEK293T cell lines and 2.5µg/ml in MEF cell lines. In general, WT refers to the DOX induced unmutated MEK1 tagged with the BirA ligase (TurboID) and a V5 tag.

4.2 Proximity dependent labeling – TurboID

Cells were grown to 80% confluency and treated with DOX 24 hours prior to experiment, inducing the expression of TurboID labeled constructs. 500µM of biotin was added to the plates and returned to the incubator for 10 min. Following incubation, cells were kept on ice. Cells were washed thrice in ice-cold PBS and pelleted in 1.5ml Epis.

4.3 Immunoblotting

Cells were washed twice in ice-cold PBS and lysed by resuspending in RIPA buffer (1% Triton X-100, 0.1% SDS) and incubated on a rotating wheel at 4°C for 15 minutes. Following incubation, samples were centrifuged at 15,000 RCF and supernatant was collected. Protein concentration was measured using Thermo Scientific BCA kit. Cell lysates (10 – 15 µg protein) were resolved by SDS-PAGE, 10% gels in combination with protein size markers (Page Ruler Plus™, prestained protein ladder, Thermo Scientific). Proteins were transferred in an overnight wet transfer (0.25M Tris, 1.92 M Glycine, 10% ethanol) onto an activated PVDF membrane (Immobilon-P, Millipore). Following the transfer, membranes were blocked with 5% non-fat dry milk in TBST (250mM Tris, 1.5M NaCl, pH 8.0 with 0.1% Tween 20) for 1 hour. Post blocking, membranes

were rinsed and incubated in primary antibody overnight at 4°C. Following primary incubation, membranes were washed 3x5min in TBST and then incubated in secondary antibody (HRP-linked) for 1 hour at room temperature. Following incubation, membranes were washed in 3x5min in TBST and then developed in chemiluminescent substrate (SuperSignal™ West Pico/Femto) and visualized using a Bio-Rad ChemiDoc.

4.4 Seahorse metabolic flux assay

Agilent Seahorse 96-well plate was coated with fibronectin. $2x10^4$ cells were seeded in normal medium with total volume of 100µL in each well. Cells were treated with DOX and incubated under normal conditions for 24 hours. For overnight Trametinib treatments, 30nM of Trametinib was added 2 hours post seeding. Pyruvate uptake inhibitor was added to the medium 2 hours prior to the experiment. Seahorse cartridge was placed in sterile water and warmed overnight in a humid CO_2 -free incubator. On the day of the experiment, the cartridge was placed in calibration medium, again in a humid CO_2 -free incubator. 2 hours prior to experiment, DMEM was changed to Seahorse medium containing 10mM glucose, 1mM Glutamate, 2mM pyruvate. Post medium change, Seahorse plate was placed in prewarmed Cytation™ and bright field images of wells were collected. Simultaneously, Seahorse cartridge was prepared for the MitoFlux assay by pipetting Oligomycin (1µM final concentration), FCCP (2µM final concentration), and Rotenone / Antimycin (0.5µM final concentration) and Hoechst (3µM final concentration) into the four ports. Cartridge and plate were inserted into Seahorse XF Analyzer and assay was conducted using three injections of each reagent followed by three measurement intervals. Following the assay, Hoechst stain was incubated for 45 minutes. Cell plate was transferred back to Cytation™ and fluorescent images were collected to normalize data.

4.5 Flow cytometry

Flow cytometry experiments were conducted using BD LSRFortessa™ and results were analyzed using FlowJo 10.6.1 software.

MEF cells intended for analysis were seeded 48 hours prior to experiment in 3cm petri dishes, $5x10^5$ cells/plate. 24 hours prior to experiment, 2.5µg/ml DOX was added. On day of experiment, 50nM of MitoTracker Green, 200nM TMRE, and 5 µM CellRox was added and incubated in darkness at 37°C for 30 min. To control for TMRE signal, CCCP was added 3 hours prior to TMRE

staining. Post incubation cells were washed 1x in ice-cold PBS and trypsinized. Trypsin was deactivated by adding DMEM, followed with spin washes by centrifuging at 300 RCF. Post centrifugation, cells were washed 2x in ice-cold PBS and resuspended in fixable viability dye. After 20 min incubation, cells were washed 2x in PBS and resuspended in ice-cold PBS. 50.000 cells were analyzed in each experiment. Representative gating for analysis is seen below:

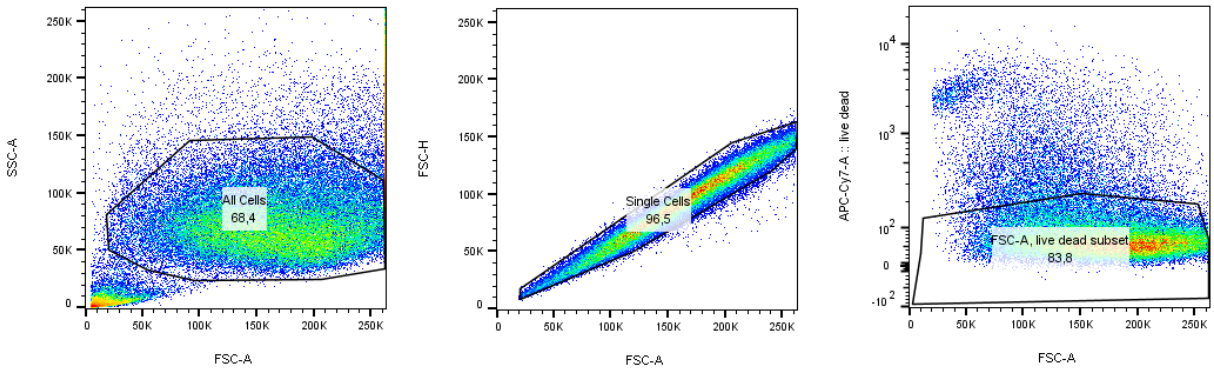

Figure 8 | Representative gating for flow cytometry experiments

4.6 Gradient centrifugation

1x10^8 cells were pelleted, frozen in liquid nitrogen, and stored at -80°C until day of isolation. Cells were resuspended in 5ml PBS, pelleted and then resuspended in 5ml homogenization medium. Suspension was dounced with tight-fitting Dounce for 20 strokes. Following douncing, homogenate was centrifuged at 1000 RCF for 10 min. Supernatant was removed and saved. Resulting pellet was resuspended in in 3ml homogenization medium and homogenized with 3 strokes in loose-fitting Dounce. Homogenate was again centrifuged at 1000 RCF for 10 min. Supernatant was removed and combined with previously collected supernatant. Combined supernatants were centrifuged at 12,000 RCF for 15 min. Resulting pellet was resuspended in 3ml PBS, homogenized with loose-fitting Dounce and centrifuged at 12,000 RCF for 15 min.

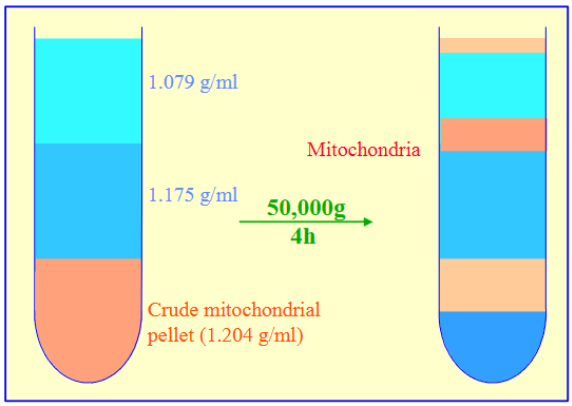

Figure 9 | Representative scheme for gradient loading as provided by OptiPrep. Gradients were bottom loaded based on protocol from Zhou, 2001.

OptiPrepTM Application Sheet S14 9th edition, January 2020

Pellet was resuspended in 1.5ml of homogenization solution. 1.4 ml of suspension was diluted with 3.6ml of 50 % iodixanol. Entire 5ml was loaded into 14ml Beckmann polypropylene centrifuge tube (REF: 331374) followed by gradients containing 27% iodixanol and 14.5% iodixanol respectively (Zhou et al., 2001).

Balanced bucket rotor were loaded with samples and attached to precooled Beckmann SW 41 Ti rotor. Centrifugation was conducted at 50,000 RCF for 4 hours. Following centrifugation, gradients were isolated and collected in epis. Gradient containing mitochondria was diluted in homogenization medium and centrifuged at 15,000 RCF for 15min. Resulting pellet was resuspended in 300µl of homogenization solution and stored at -80°C.

4.7 qRT-PCR

mRNA was collected from mRNA isolation kit (Macherey-Nagel). Isolations were completed following manufacturer's protocol. Product mRNA was resuspended in 40µl of NF ddH_2O. mRNA concentration was measured using NanoDrop™ and stored at -80°C. cDNA was produced from 400ng of mRNA first by incubating with 1µg of Oligo(dt) (Thermo Scientific SO132) at 70°C for 10 min. Samples were transferred to ice and combined with 4µl RT Buffer, 2µl ddH_2O, and 2µl dNTPs. Samples were heated to 37°C for 5 min before adding 1µl of Reverse Transcriptase (Thermo Scientific EP0441) and incubating at 42°C for 60min. Post incubation, samples were heated to 70°C to denature enzymes and stop the reaction. Resulting product was resuspended in 200µl of NF ddH_2O. cDNA samples were stored at -80°C. qPCR was completed follow protocol for NEB Sybr Luna® with 250nM of forward and reverse primer and 5µl of cDNA sample per reaction well. qPCR settings used a maximum temperature of 95°C followed by 40 cycles oscillating between 60°C and 95°C with 30 second and 15 second time intervals respectively (NEB qPCR Protocol). Experiments were done in biological triplicates. Relative fold change of gene expression was normalized using the housekeeping gene Hprt and calculating $2e\text{-}\Delta Ct$ for each gene of interest.

4.8 Statistics

GraphPad Prism software was used to analyze data. P values were calculated using Anova multi-comparison analysis and values below 0.05 indicate significant differences. Experiments were performed in triplicates unless otherwise noted.

5. Results

5.1 Aims of Thesis

The project began with a screen and with the objective to elucidate novel interactors of MEK1, indicating perhaps moonlighting functions of the penultimate node in the MAPK pathway. Variants of MEK1 containing specific point mutations, as well as the TurboID system, were generated by Georg Vucak and expressed via a DOX inducible system in HEK 293T cells and MEF cells. Proximal proteins to the variants of MEK1 (WT, T292A, T292D, N78G, S218/222A, S218/222D, Q56P, K57E, K57N) were labeled with biotin in triplicates and extracted using streptavidin beads. Subsequently, these samples were submitted to the Max Perutz Labs Mass Spectrometry Facility to determine the nature of the proximal proteins. Sebastian Didusch analyzed the data produced by G. Vucak's screen, using a TurboID labeled GFP as a control.

The interactome generated from the screen indicated interactors in various aspects of cell biology. An enrichment of mitochondrial proteins was observed in the screen, which became the scope of this project. While it is known that proteins associated with the mitochondria have the propensity to be false positives in BioID screens due to carboxylase activity, the magnitude and disparate of mitochondrial proteins observed in the screen sparked interest. Some of the top mitochondrial hits can be seen in the image below, exemplifying the functional diversity of proteins found to be in the proximity of MEK1 variants. As the majority of the hits were associated with the Q56P genotype, we sought to investigate differences in mitochondria mass, functionality and metabolism between this mutant, MEK1 WT, and MEK1 KO. Further, we attempted to assess protein content of mitochondria isolated from the different genotypes to determine if MEK1 is entering the mitochondria as the results in the proximity screen could imply.

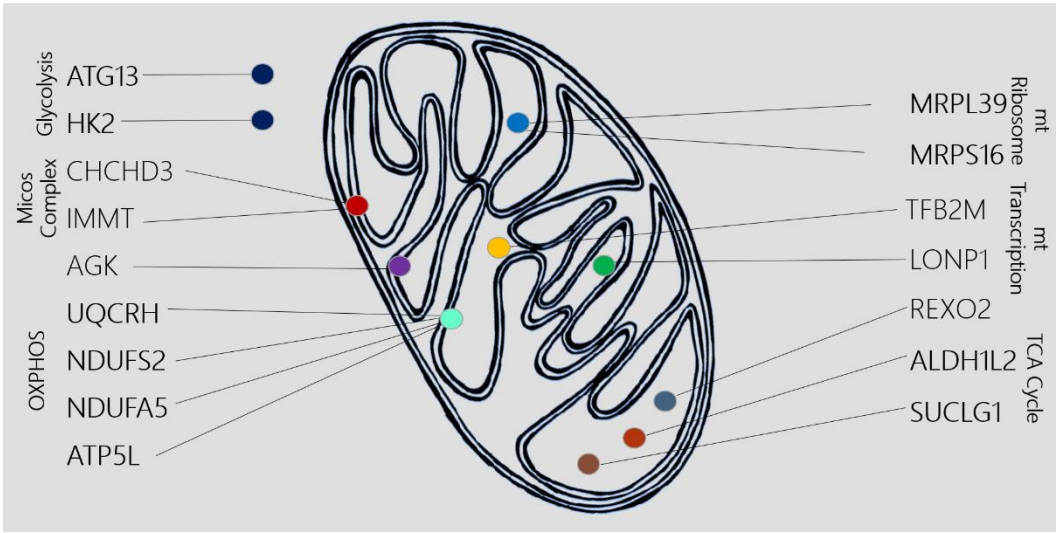

5.2 Phosphorylation activity of MEK1 mutants and interpretation of PDL-mass spectrometry screen

Proximity dependent labeling via the TurboID system was induced in wild type (WT) HEK293T cell lines including various MEK1 genotypes, as well as MEK2, MP1 (scaffold protein MEK Partner 1), PTEN (Phosphatase and Tensin Homolog), and GFP (Green Fluorescent Protein), tagged with TurboID. For the sake of this work and the scope of the project, focus will be given to the different MEK1 mutants. Lysates of the various genotypes were collected in triplicates by G. Vucak and biotinylated proximal proteins were extracted from the lysates and submitted to mass spectrometry (MS) analysis. In order to better understand the phosphorylation profiles of the submitted samples, analysis using western blotting looked at critical signaling nodes associated with MAPK signaling. A representative blot from one of the triplicates is seen in Figure 10.

Immunostaining confirmed the various mutations of MEK1. The mutated forms of MEK1 run around the 100 kDa marker due to the addition of BirA ligase and a V5 tag. Investigating the phosphorylation at RDS shows the S218/222A+D mutations were effectively introduced into the protein, as the ability to be phosphorylated is eliminated with the loss of serine at these sites. Similarly, the ERK feed back loop mutations, T292A+D, effectively hindered phosphorylation at T292 site, indicating the threonine is no longer present at residue 292. The phosphorylation of upstream BRAF was unaffected by the various MEK1 mutants, indicating that upstream BRAF activity was not modulated by the various mutations. The same is true for AKT activation, as the phosphorylation of AKT at serine 473 showed insignificant differences cross mutants, indicating AKT activation is not influenced by the different MEK variants. Activation of downstream ERK was indicated by the phosphorylation at threonine 202 / tyrosine 204 (ERK1) and threonine 185 / tyrosine 187 (ERK2) and indicated on the blot as IB: pERK. As expected, the constitutively active mutation of MEK1 (S218/222D) showed a robust increase in downstream ERK phosphorylation, indicating the aspartic acid substitution did effectively mimic phosphorylation and activation from upstream RAF. Interestingly, two of the disease associated mutants also showed robust increases in pERK compared to the WT. Q56P and K57N have been shown to arise in different cancer types (Murugan et al., 2009), indicating the resulting increase in ERK phosphorylation associated with these mutations could play a role in driving cell proliferation.

In order to further investigate the observed increase in pERK signaling, a starvation protocol followed by epidermal growth factor (EGF) stimulation was conducted to determine the effects of both starvation and stimulation on the pERK phenotype. HEK293T cells with DOX induced

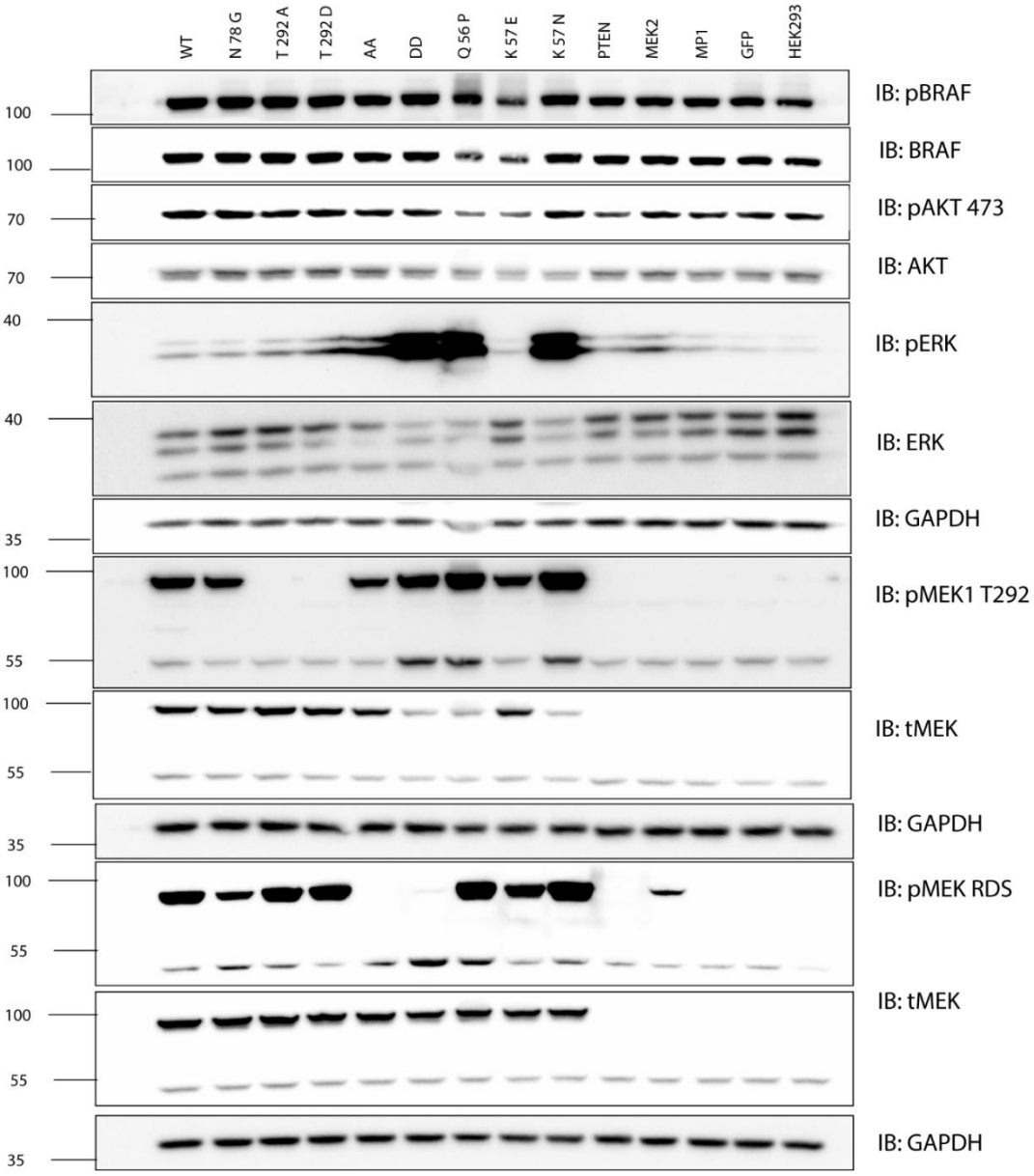

Figure 10 | ***Western Blot Investigation of MEK Variants in HEK293T Cells*** Blots confirm the induction of the indicated MEK1 mutants. Substitutions of aspartic acid for serine at RDS induces constitutive activation of the canonical pathway seen by the pERK readout. Interestingly, two other disease mutants induce a similar phenotype, increasing the activation of downstream ERK.

MEK1 mutations were kept over night in starvation medium (normal medium with 0% FCS) and were then stimulated with EGF (100ng/ml) for four different durations (0, 5, 30, 60 minutes), as well as a non-treated (NT) control. Seen in Figure 11, WT MEK1, as well as most of the mutants, showed an expected phenotype. The pERK signal was weak following starvation, strong 5 minutes post EGF stimulation, and again weak 30-60 minutes post stimulation. The S218/222D, Q56P, and K57N genotypes however were unaffected by both starvation and stimulation conditions, instead high levels of ERK phosphorylation was observed at all time

points. These results substantiated the robustness of ERK activation associated with these mutations.

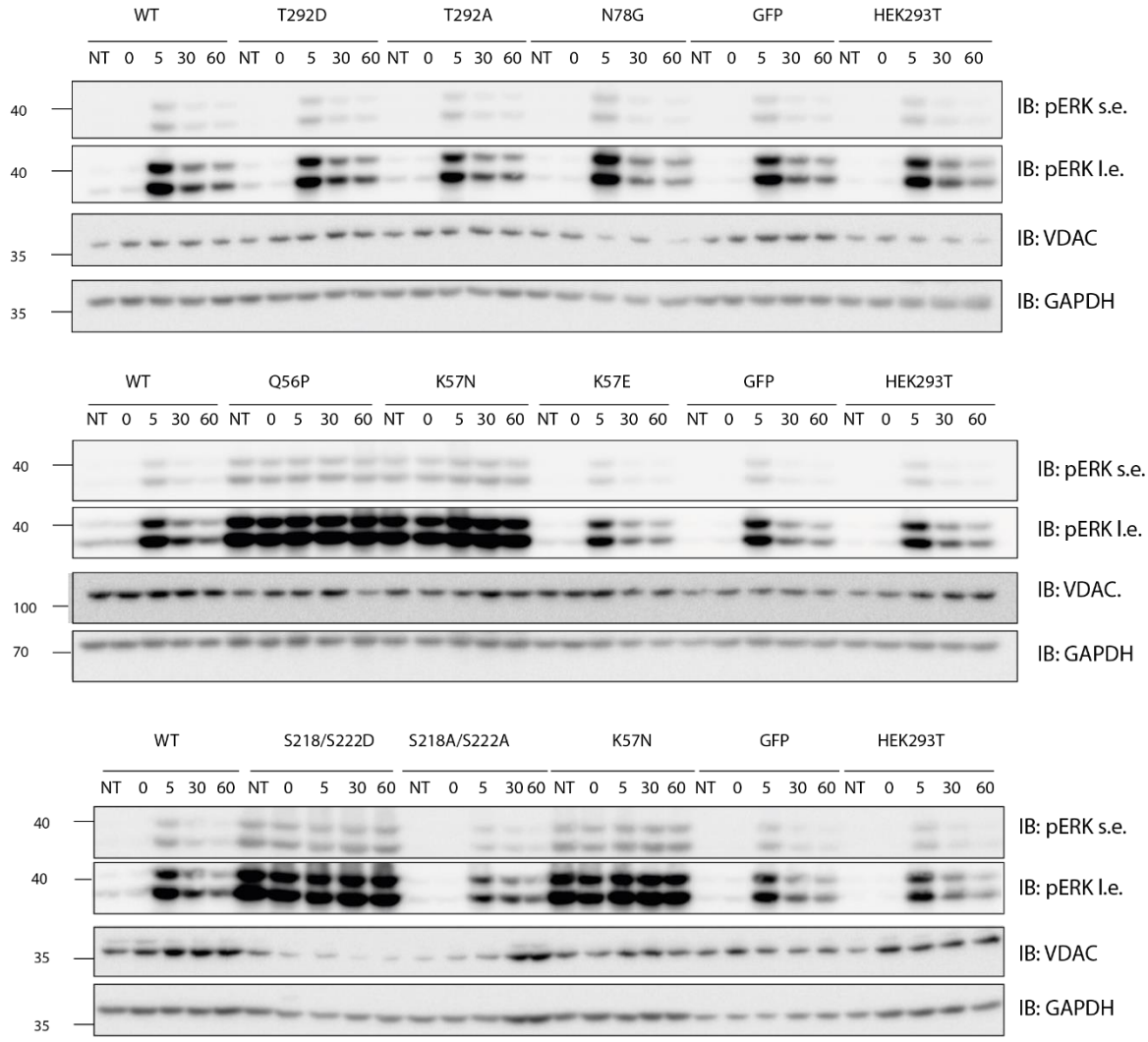

Figure 11 | ***Starvation & EGF Stimulation of HEK 293T MEK1 Constructs*** The observed increase in pERK signal associated with Q56P, K57E, and S218/222D was unaffected by starvation and EGF stimulation, differing significantly form the other variants of MEK1. Images of pERK signal were taken at short and long exposures to better visualize differences in protein abundance between the different samples. NT represents starvation without EGF stimulation. Time points 0, 5, 30, 60 represent the interval between EGF stimulation and cell lysis. GAPDH and VDAC were used as loading controls.

5.3 Flow cytometry assessment of mitochondrial mass and functionality

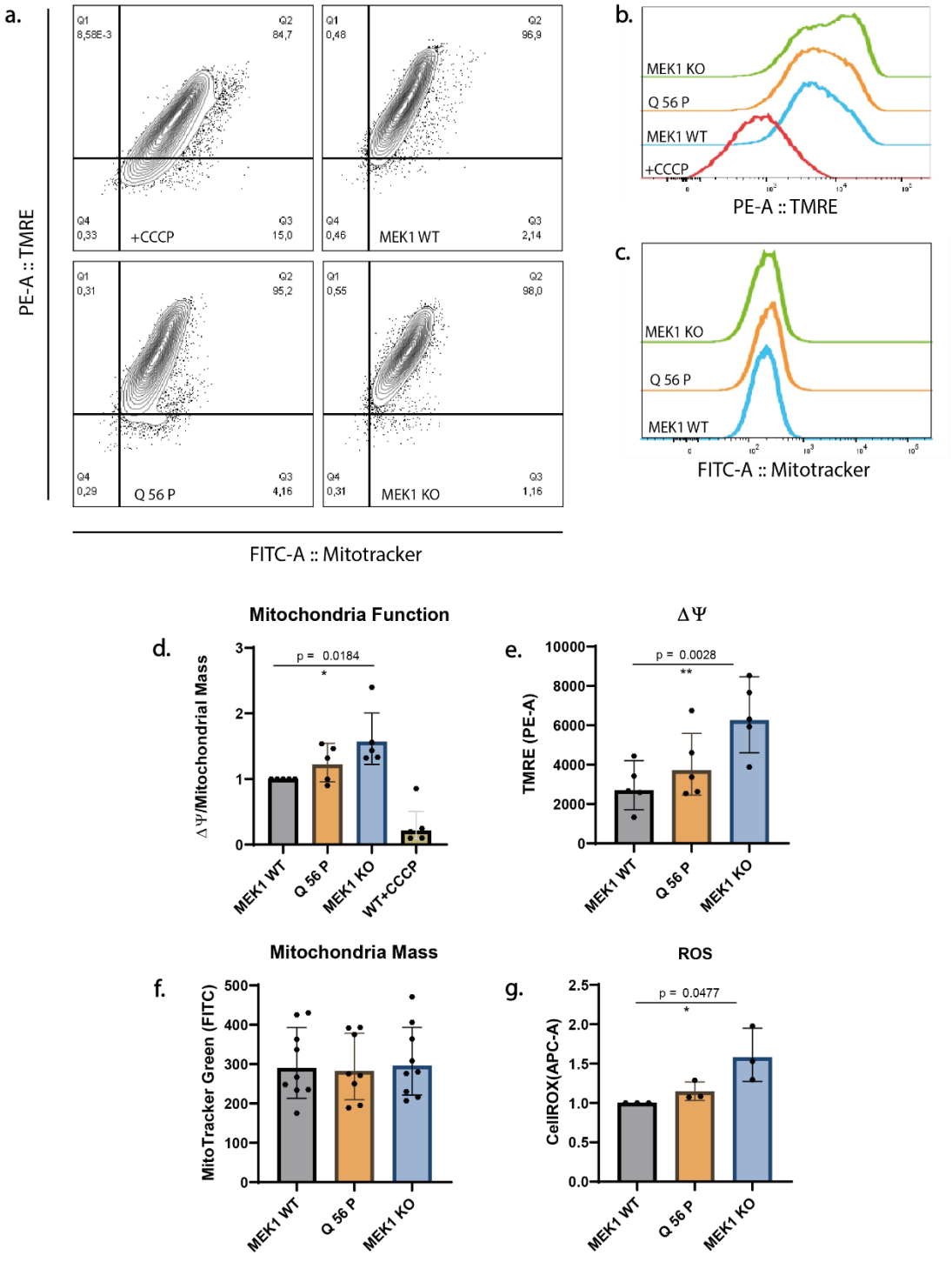

Figure 12 | ***Flow Cytometry Analysis of Mitochondria*** A) Comparison of TMRE vs MitoTracker signal in MEK1 variants. B,C) Representative peaks of TMRE and MitoTracker signal. D) Comparison of mitochondria functionality n = 4, star represents significance between MEK1 WT and MEK1 KO. E) TMRE signal in MEK1 genotypes n = 5. F) MitoTracker signal n = 9. G) Comparison of ROS production between MEK1 genotypes n = 3.

The results of the PDL screen indicating numerous mitochondrial protein hits associated with the Q56P genotype led us to question if the mitochondria load was equal between the different genotypes. If the Q56P mutant simply generated more mitochondria, it could explain the increase in proximally labeled proteins associated with this mutant. To investigate this, the mitochondria of the three genotypes (MEK1 WT, Q56P, MEK1 KO) in MEF cells were labeled with MitoTracker green and the fluorescent signal was measured using flow cytometry. The resulting peaks associated with MEK1 WT, Q56P, and MEK1 KO can be seen in Figure 12 C. While extremely minimal shifts in mitochondrial mass were observed in individual experiments, numerous replicates of the experiment allowed us to conclude that the mitochondria load between the three genotypes was equal. Quantification of all experiments can be seen in Figure 12 F.

Knowing that the number of mitochondria between the three genotypes was constant allowed us to pursue the idea that the differences in mitochondrial protein proximity observed in the PDL screen was due to protein interactions, and not simply an increase in mitochondria mass, which would lead to increased mitochondrial proteins in the proximity of the Q56P mutant. To further investigate the differences in the mitochondria in the three genotypes, we used a TMRE (Tetramethlrhodamine, Ethyl ester) stain to provide us with a readout for mitochondria health. The mitochondria transmembrane potential ($\Delta\Psi$) is sustained via the proton gradient established by the ETC to produce ATP. The membrane potential of healthy mitochondria resides approximately at -180mV. TMRE is a positively charged dye that has a strong affinity for the highly negative mitochondria membrane. Thus a stronger TMRE signal correlates to a more negative $\Delta\Psi$, and vice versa. TMRE can be correlated to the efficacy of the electron transport chain, as the shuttling of electrons by Complex I – IV is essential to pump protons in the inner membrane space, which gives rise to $\Delta\Psi$ (Crowley et al., 2016).

MEK1 variants were co-stained with MitoTracker green and TMRE. Mitochondria function can be determined by dividing the TMRE signal by the MitoTracker signal, essentially normalizing the $\Delta\Psi$ to the mitochondria mass. As a control, CCCP (Carbonyl cyanide m-chlorophenyl hydrazone) was administered to the MEK1 WT. CCCP is an uncoupler and disrupts the proton gradient across the IMM. As such, the CCCP signal represents severely unfunctional mitochondria. TMRE and MitoTracker signal were assessed in MEK1 variants as well as in the CCCP control using flow cytometry. Looking at the peaks associated with the TMRE signal in Figure 12 B, MEK1 KO showed an increase in TMRE signal, where MEK1 WT and Q56P remained consistent with one another. Figure 12 A shows comparative gating of TMRE and MitoTracker. The shift associated with CCCP is clear in the first panel, however the shift between the different

genotypes was not as evident, with only MEK1 KO showing a significant increase in mitochondria functionality Figure 12 D.

CellROX was used to measure ROS production in the MEK1 variants. Cells were stained with CellROX and analyzed again using flow cytometry. In line with the increase in mitochondria functionality associated with MEK1 KO, an increase in ROS was also observed. As ROS is produced through the activity of the ETC (Figure 7*)*, increased ETC activity should correlate to increased ROS production. Since MEK1 KO has a stronger TMRE signal, Figure 12 E, which corresponds to increased ETC activity, it is in line that MEK1 KO also shows increased ROS production.

Flow cytometry assessment of mitochondria in MEK1 variants pointed to differences associated with the ablation of MEK1 compared to the MEK1 WT. Substantial differences associated with the disease mutant Q56P and MEK1 WT were however not observed.

5.4 Investigation of metabolic profiles of MEK1 mutants

To investigate the metabolism of the different MEK genotypes, Agilent flux technology was used. The Seahorse XFe96 analyzer uses the sensitivity of twin fluorophores to detect changes in oxygen and pH in the experimental system. This oxygen detecting fluorophore provides a readout for oxygen consumption rate (OCR), correlating to OXPHOS activity. The pH sensitive fluorophore determines extra cellular acidification rate (ECAR), correlating to glycolysis, as increased production of lactic acid is the main influencer of extracellular pH. The measurements take place in a 7µl microchamber that is created when the fluorophore containing probe is lowered into the well on the 96 well plate. The small volume increases sensitivity, measuring subtle changes in metabolism that result from the experimental conditions. As glycolysis is the physiological response to hypoxia, the Seahorse flux protocol allows for comparative measurements across genotypes to the glycolytic response associated with hypoxic conditions. This is achieved through the microchamber. When the fiberoptic probe from the cartridge is lowered into the well of the plate, a microchamber is formed. As oxygen is consumed by the cells in the plate, real-time measurements can be collected, correlating to the cellular response to the hypoxic environment. To probe mitochondria metabolism, the MitoStress test was used to determine basal and maximal respiratory capacity correlating to ETC efficacy. The injection protocol for the assay can be visualized in Figure 13.

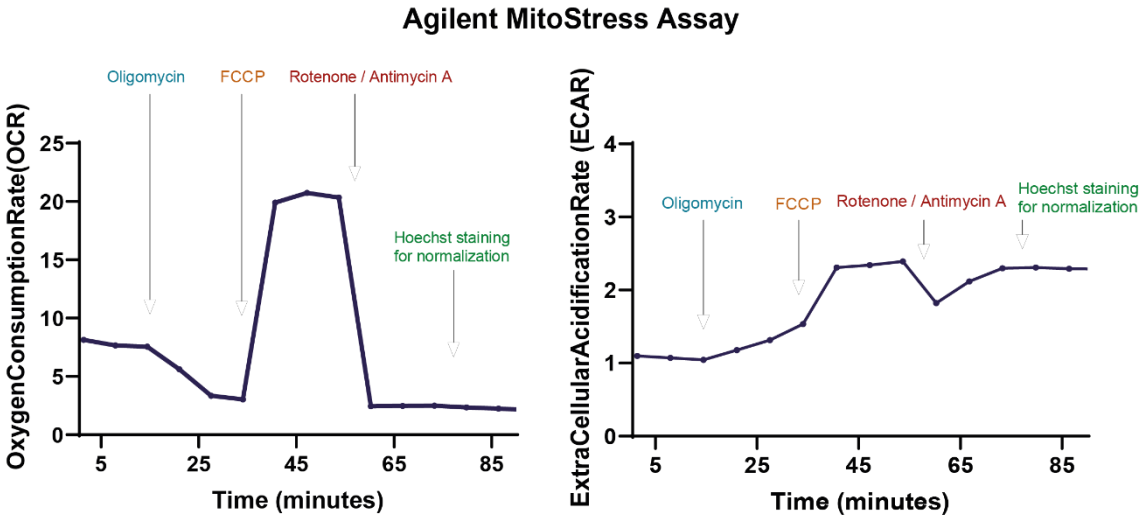

Figure 13 | *Agilent MitoStress Assay* Oxygen consumption rate and extra-cellular acidification rate are measured in the Seahorse flux analyzer. Micro injections of compounds blocking specific components of the ETC are made, starting with oligomycin (ATP synthase inhibitor), FCCP (IMM uncoupler), Rotenone + Antimycin (Complex I + Complex III inhibitor), and Hoechst (Fluorescent stain for well normalization). Simultaneously the machine measures changes in oxygen and pH levels, providing a readout for OXPHOS and Glycolysis activity. Injections are made three times, followed by a 3 minute measurement period.

The initial investigation of metabolism looked at all 9 variants of MEK1. MEF cells were used because they remained adherent through the numerous wash steps required in the MitoStress protocol. OCR and ECAR for the 9 genotypes were determined, as seen in Figure 14. Robust differences in OCR and ECAR were not observed when comparing the 9 different MEK1 variants. Based on the results of the PDL screen and the lack of significant differences between OCR and ECAR between the different genotypes at steady state, we decided to focus further flux assays to compare MEK1 WT, Q56P, and MEK1 KO.

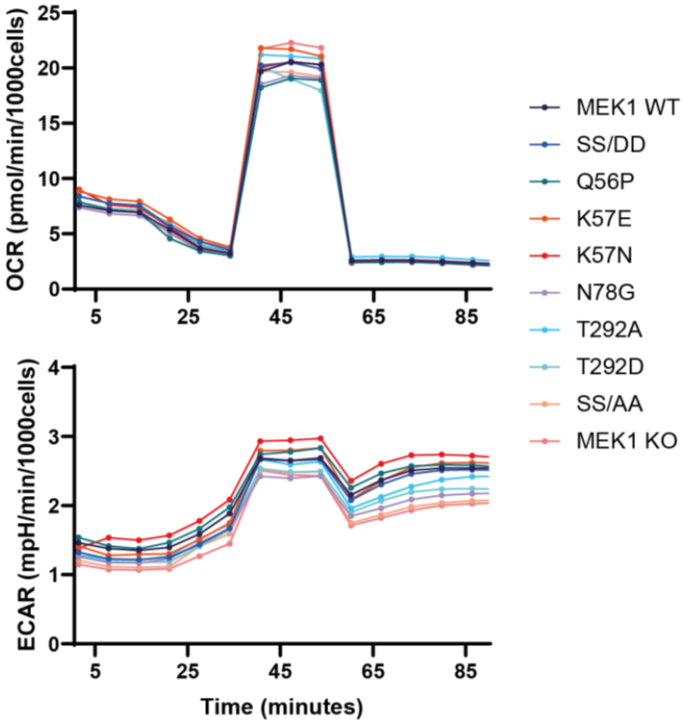

Figure 14 | *OCR & ECAR Comparison of MEK1 Variants*

Assessing the metabolism of the three genotypes at steady state indicated MEK1 KO has significantly increased maximal OCR and decreased maximal glycolysis compared to MEK1 WT, Figure 15. Maximal refers to the first measurement following the injection of FCCP at the 40 minute timepoint. Basal refers to the measurement before the first oligomycin injection at the 9 minute timepoint. While Basal levels of OCR were equal between all three variants, ECAR was significantly less in MEK1 KO compared to MEK1 WT. MEK1 KO had a consistently lower ECAR throughout the duration of the experiment, indicating that there is a reduction of glycolytic metabolism in MEK1 KO. As glycolysis and OXPHOS are in balance with one another, it follows suit that MEK1 KO showed an increase in maximal OCR compared to MEK1 WT, indicating ETC machinery capable of supporting energy deficits resulting from reduced glycolytic activity. Further, the TMRE staining in Figure 12 E substantiates the increase in OCR observed in MEK1 KO, as a stronger TMRE signal is linked to increased ETC activity (Little et al., 2020)

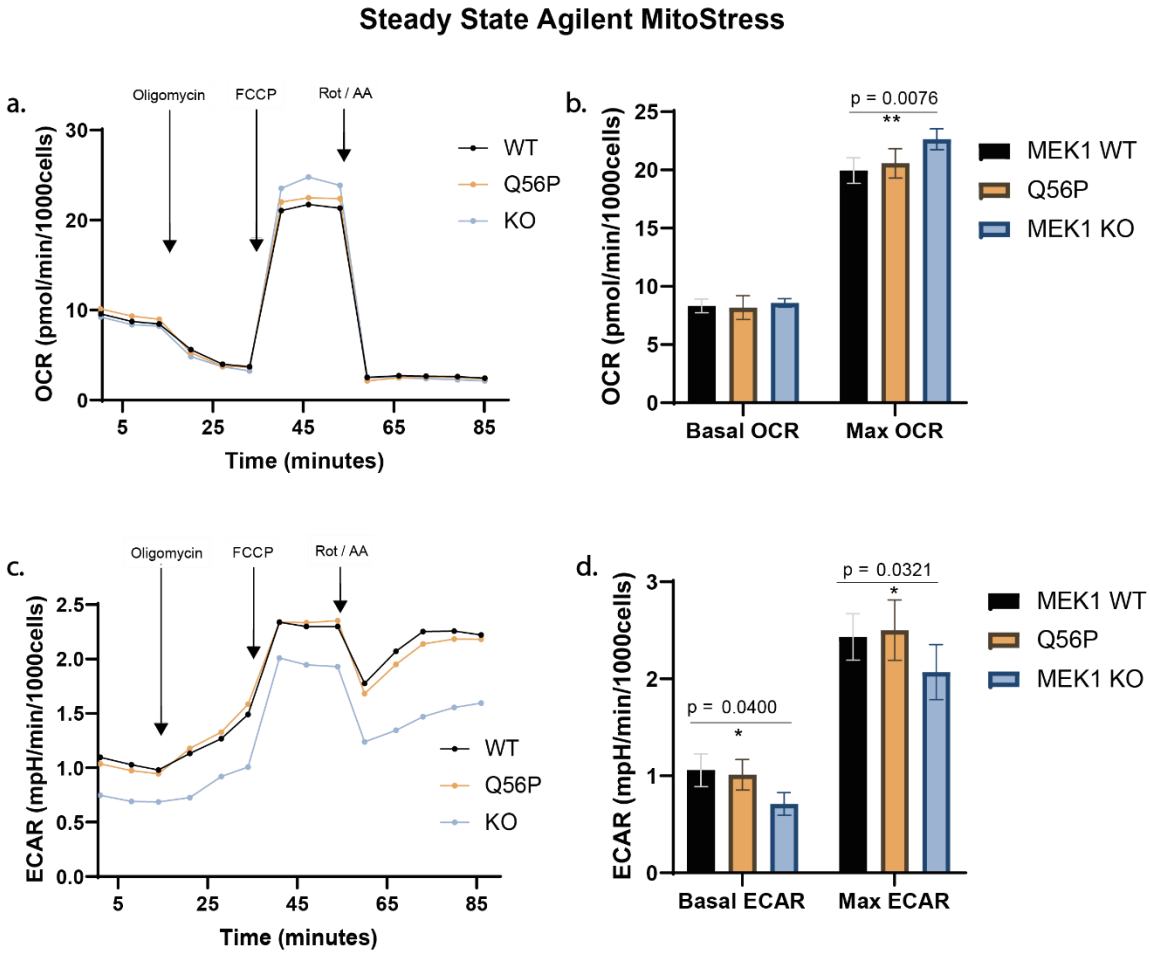

Figure 15 | *Steady State OCR & ECAR in MEK1 WT, KO, & Q56P* A) OCR measurements were made during the MitoStress protocol, indicating MEK1 KO has a significantly increased maximal OCR (B). C) ECAR measurements during MitoStress protocol indicate MEK1 KO has reduced ECAR following all injections. D) Significant decrease in ECAR in MEK1 KO compared to MEK1 WT can be visualized at both basal and maximal levels.

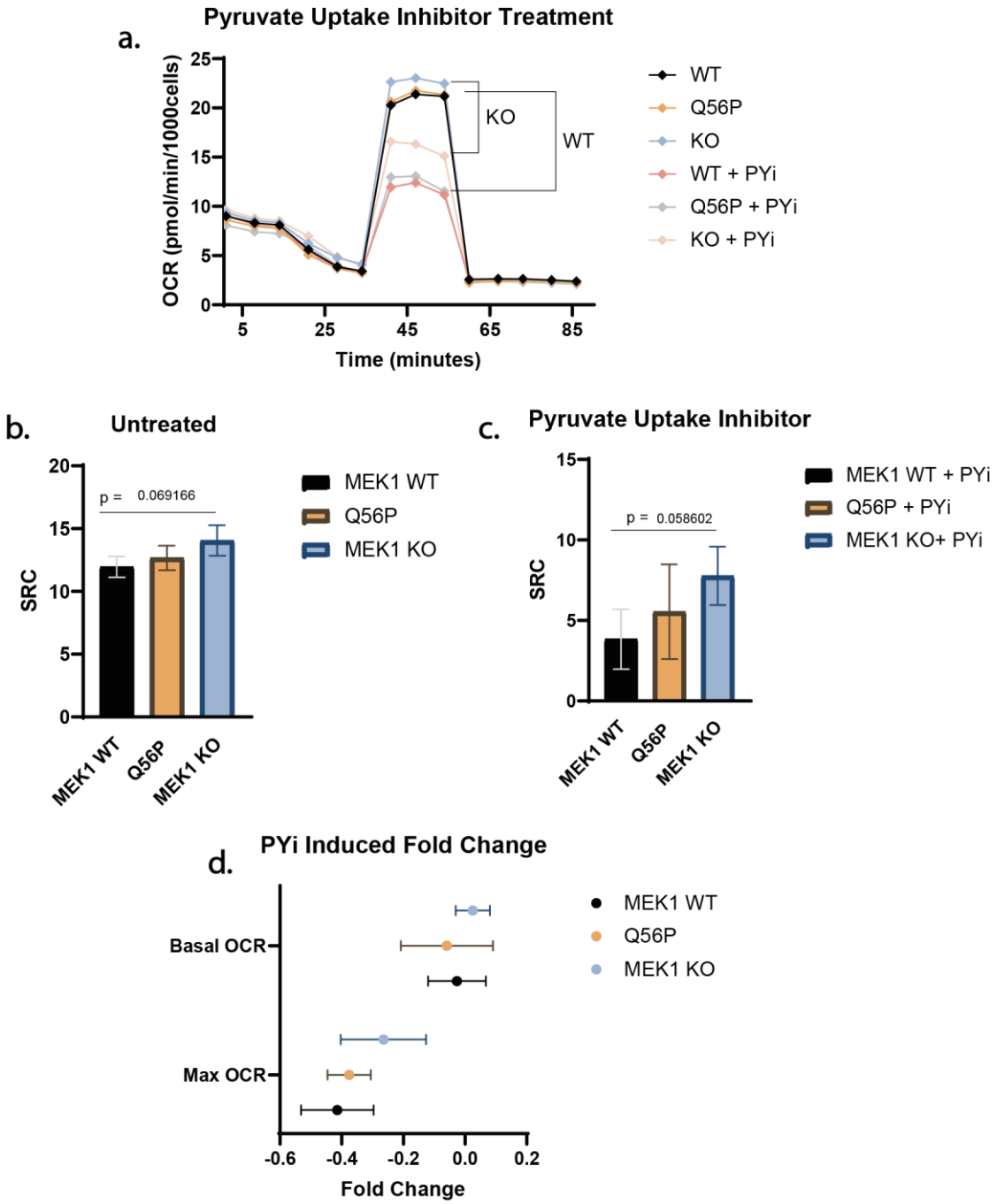

Figure 16 | *Effects of Blocking Pyruvate Uptake on OCR* Blocking the uptake of pyruvate into the mitochondria with a pyruvate uptake inhibitor (PYi) induces a reduction in maximal OCR as depicted in (A)**.** Spare respiratory capacity (SRC) decreased in all genotypes after PYi treatment (B,C) however no significant differences between the different genotypes arose from PYi treatment. Looking at the fold change associated with PYi treatment (PYi treated – untreated / untreated), the PYi induced a shift in MEK1 KO at maximal OCR that was less robust compared to MEK1 WT and the Q56P mutant. This shift however is only a trend and not statistically significant.

To probe the glycolytic shift and the increased maximal OCR observed in MEK1 KO, pyruvate uptake into the mitochondria was blocked using a pyruvate uptake inhibitor (PYi, UK5099 | Mito Fuel Felx Kit, Agilent). Blocking the uptake of pyruvate deprives mitochondria of a critical substrate for the TCA cycle. Acetyl-CoA production is stunted, reducing the production of citrate from oxaloacetate and decreasing the production of critical ETC cofactors, NADH and $FADH_2$. In all three genotypes, maximal OCR was reduced upon PYi treatment, Figure 16 A. The spare respiratory capacity (SRC) is the difference between maximal OCR and basal OCR. Comparing SRC indicates differences in OXPHOS capacity. MEK1 KO has a higher SRC in both untreated and PYi treated conditions, however the significance of SRC increase compared to MEK1 WT becomes greater under PYi treatment, Figure 16 B,C. This is further seen when comparing the fold changes associated with PYi treatment for the three genotypes, Figure 16 D. The fold change was determined for maximal and basal OCR by ((Y-X)/X), where Y = PYi treated OCR values and X = untreated OCR values. At basal levels, minimal fold change was observed, oscillating around 0. This is seen also in Figure 16 A, as PYi treatment does not induce a drop in basal OCR, indicating all genotypes are able to compensate for the inhibition of mitochondria pyruvate uptake. When the IMM is uncoupled following FCCP injection and OCR is at a maximum, a trend was observed that MEK1 KO has a smaller fold change (-0.25) compared to MEK1 WT and the Q56P mutant (-0.4, -0.35, respectively), indicating MEK1 KO is more resistance to compromised OXPHOS associated with PYi treatment. This could be because other metabolic pathways that feed the TCA cycle, such as glutaminolysis or FAO, may be enriched in MEK1 KO compared to MEK1 WT, providing critical cofactors to allow ETC components to function and consume oxygen. In all, these data are not statistically significant and represent interpretations and hypotheses of observed trends. Further extensive metabolic experiments must be completed to determine if MEK1 KO does correlate to increased glutaminolysis or FAO.

Because MEK1 KO showed a sustained decrease in glycolysis compared to MEK1 WT and the Q56P mutant, we wanted to probe the idea that MEK1 was responsible for this shift in metabolism. To do this, we chemically inhibited MEK1 using trametinib. Because we wanted to induce metabolic changes, a 24 hour treatment of 30nM was chosen based on its clinical relevance (Selvasaravanan et al., 2020). Treating the genotypes with trametinib induced a shift in ECAR that was consistent across all samples. The shift was observed at both basal and maximal ECAR and can be visualized in Figure 17 A-C. Treating MEK1 WT and Q56P with trametinib caused ECAR to shift in the direction of untreated MEK1 KO, indicating that chemically inhibiting or ablating MEK1 has effects on glycolysis. However, trametinib treatment actually reduced ECAR levels below those of untreated MEK1 KO, indicating MEK1 unspecific

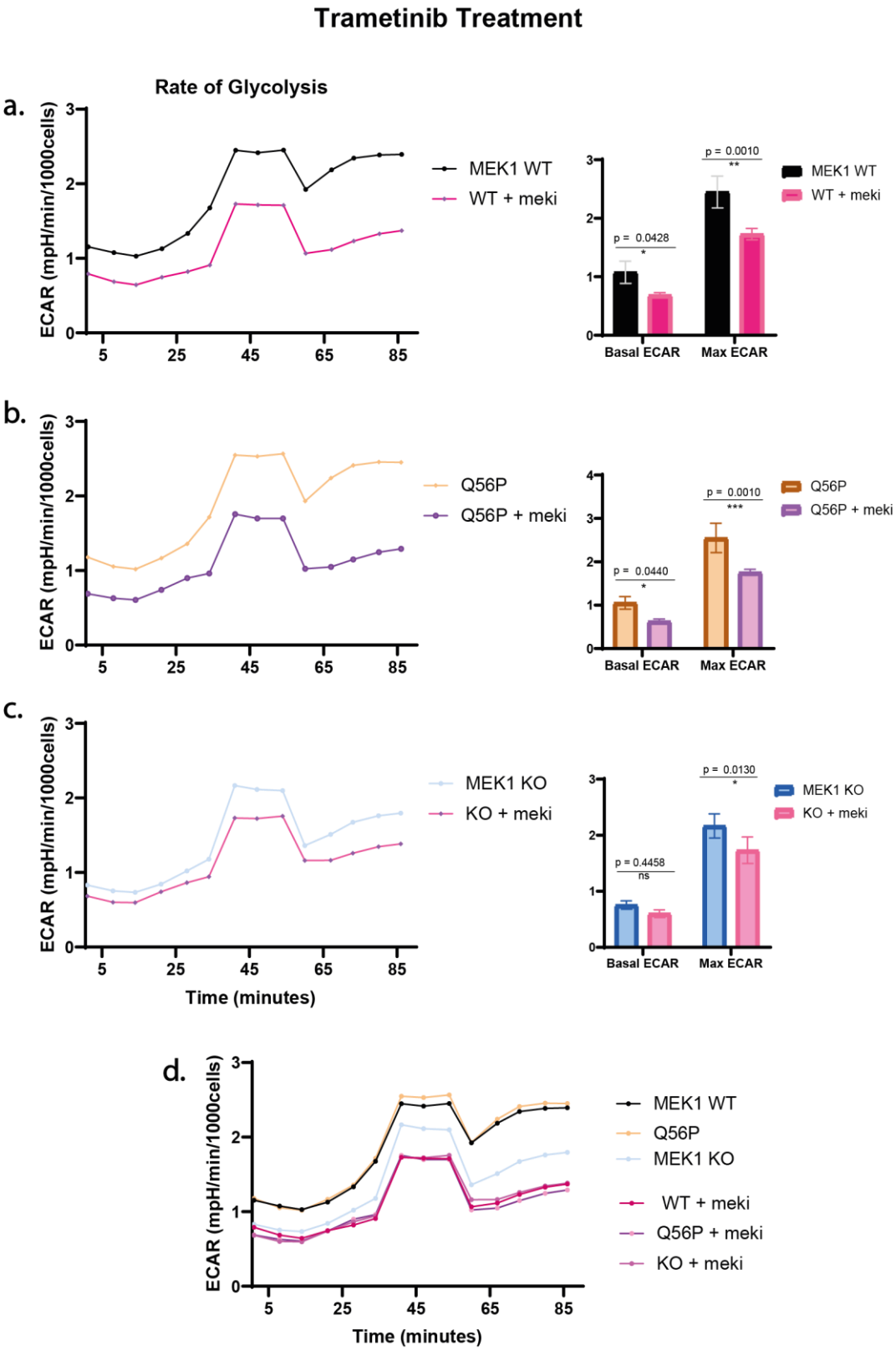

Figure 17 | *Trametinib Treatment in Variants of MEK1* Trametinib treatment in MEK1 WT and Q56P induces an ECR shift that resembles untreated MEK1 KO (A,B). Trametinib also induces a shift in MEK1 KO, however this shift is less statistically significant compared to the shift observed in MEK1 WT and Q56P (C). Comparing the three genotypes shows trametinib induces a glycolytic shift that surpasses the shift associated with MEK1 ablation. (meki = trametinib)

metabolic effects of trametinib. This was substantiated by the slight ECAR shift in MEK1 KO when treated with trametinib, Figure 17 C. The reason for this shift could be off-target effects of trametinib that target metabolism or the effect of blocking MEK1 and MEK2. Trametinib targets both forms of MEK. Because trametinib treated genotypes showed further reduction of ECAR compared to untreated MEK1 KO, this could imply that both MEK1 and MEK2 may play a potential role in regulating aspects of glycolysis and metabolism at large.

Trametinib treatment in MEF cells was visualized on western blot basis to compliment Seahorse flux data. Seen in the blots in Figure 18 A, the reconstituted version of MEK1 was effectively expressed in MEK1 WT and Q56P. Further, this blot also confirms that the knocking out of MEK1 is still effective. Looking at phosphorylation at RDS, trametinib is able to remove essentially all phosphorylation in MEK1 WT. Q56P is more resistant to the effects of trametinib on RDS compared to MEK1 WT, following suit with Q56P disease associations. Phosphorylation at T292, the site of ERK feedback, shows comparable amounts of phosphorylation in both MEK1 WT and the Q56P mutant. MEK2 is still effectively expressed in all three genotypes, which allows us to postulate that the increased glycolytic shift associated with trametinib treatment could stem from inhibition of both MEK1 and MEK2. This would explain the slight shift in ECAR observed in MEK1 KO treated with trametinib.

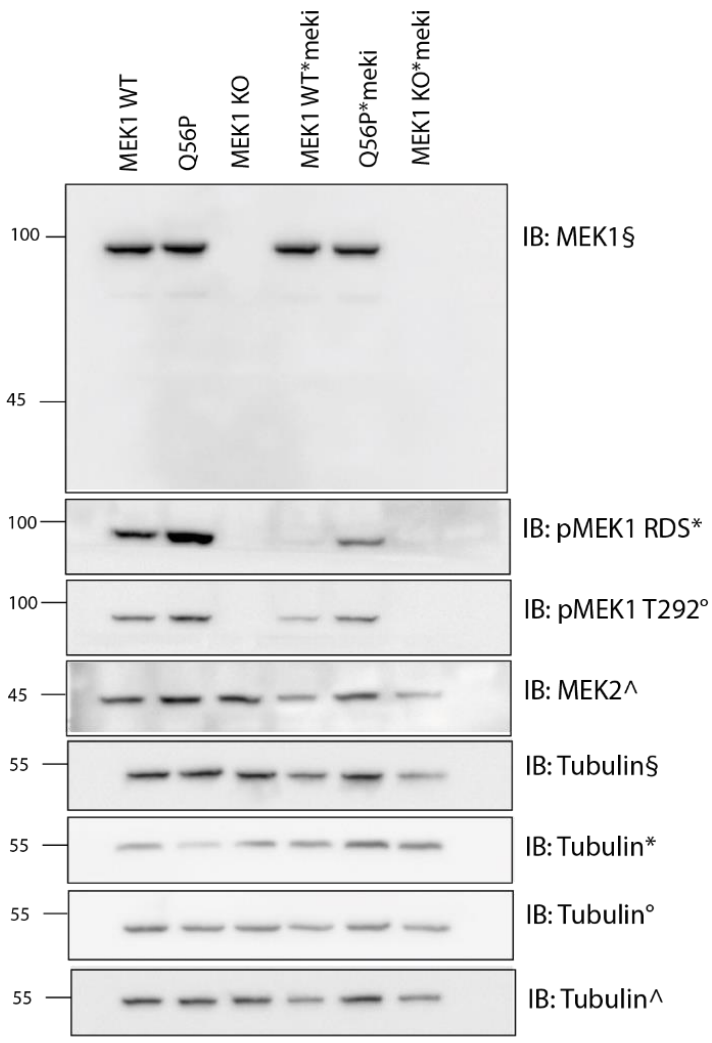

Figure 18 A | ***MEK and Critical MEK1 Phosphorylation in Untreated and Trametinib Treated State (meki = Trametinib)***

Down stream ERK activation was also investigated in both untreated and trametinib treated conditions. Seen in Figure 18 B, the robust increase of pERK in the Q56P mutant observed in

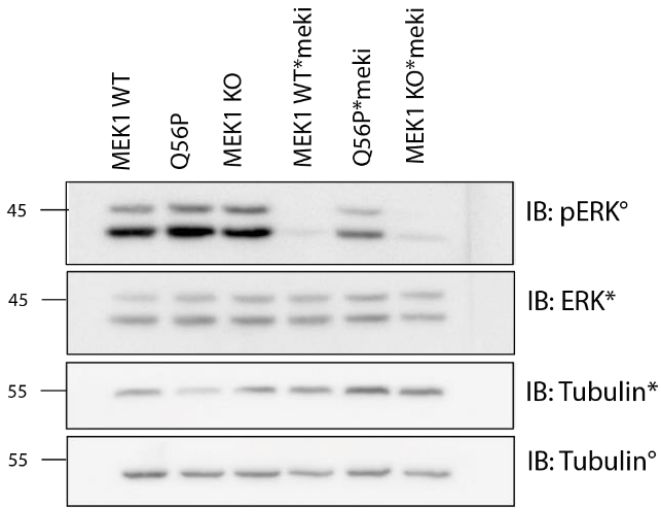

Figure 18 B | *Phosphorylation of ERK*

HEK293T cells containing the mutation was not observed in the MEF cells. While there is a slight increase in ERK phosphorylation associated with Q56P, the phenotype is not as strong in the MEF cells. Interestingly, treatment with trametinib shuts down nearly all phosphorylation of ERK in MEK1 WT and MEK1 KO, which is not the case for Q56P. Downstream ERK is still significantly phosphorylated in MEF cells containing the Q56P mutation under trametinib treatment. The difference between MEK1 WT and Q56P under trametinib treatment is interesting in regards to the ECAR results. Seen in Figure 17 A/B, MEK1 WT and Q56P display a near identical shift in ECAR. Knowing that the levels of ERK phosphorylation differs between these two genotypes could imply that this is an ERK independent ECAR shift. If the shift were ERK dependent, differences between MEK1 WT and Q56P would be expected, knowing that ERK is more active in Q56P. Since the major difference in ECAR shift arises in MEK1 KO, it could imply that MEK has a glycolytic regulatory function independent of downstream ERK activation.

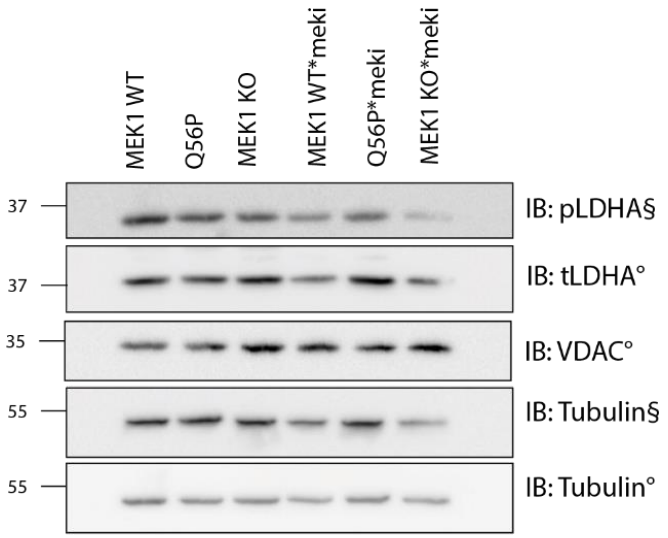

Figure 18 C | *Phosphorylation of LDHA*

Since we observed differences in ECAR, which is predominantly influenced by the excretion of lactic acid, we wanted to check the phosphorylation of LDHA (lactate dehydrogenase A). LDHA is an enzyme responsible for the conversion of pyruvate to lactate. Reduction in LDHA, as well as the phosphorylated active form pLDHA, could explain the shift in ECAR following trametinib treatment. However, seen in Figure 18C, differences in total LDHA and pLDHA were minimal.

5.5 qRT-PCR analysis of metabolic genes

To further investigate differences in MEK1 variants associated with metabolism, we looked at the gene expression of various essential metabolic genes using quantitative PCR. Amongst the metabolic genes, we were interested particularly in the genes of hexokinase, ATP synthase, NADH dehydrogenase, and succinyl-CoA ligase, as these were hits in the PDL screen. In line with the Seahorse flux experiments, we investigated gene expression in MEK1 WT, Q56P, and MEK1 KO in untreated and 24 hour trametinib treated conditions. Additionally, we looked at MEK1 KO with a TurboID GFP as a secondary control.

Results of qRT-PCR can be seen in Figure 19. In untreated conditions, little difference was observed. Only in Atp5h was an increase observed in Q56P compared to the other genotypes. Comparing untreated to trametinib treated proved to be more interesting. Expression of Atp5h was not affected by trametinib treatment, as levels of gene expression was comparable between treated and untreated conditions. Trametinib treatment reduced Hk2, Ldha, and Glut1 expression in all genotypes except for Q56P. Notably, these three genes are associated with glycolysis, lactic acid production and glucose import, respectively. While this observation was not as robust in Ldha, it is clear that gene expression of Hk2 and Glut1 is not affected by trametinib in Q56P to the extent of the other genotypes. Trametinib treatment induced an increase in Eno3 expression in all genotypes. Eno3 encodes enolase, the glycolysis enzyme responsible for the conversion of phosphoglycerate to phosphoenolpyruvate, the glycolytic step prior to pyruvate production.

While the majority of genes assessed showed little difference in expression associated with the different genotypes and the different treatments, the MEK1 mutant Q56P did show subtle differences in the expression of Atp5h, Hk2, Ldha, and Glut1. Knowing that Q56P pushes the phosphorylation of ERK could explain why expression of these genes was higher, specifically under trametinib treatment. Seen in Figure 18 B, Q56P continues to phosphorylate, and therefore activate, downstream ERK under trametinib treatment.

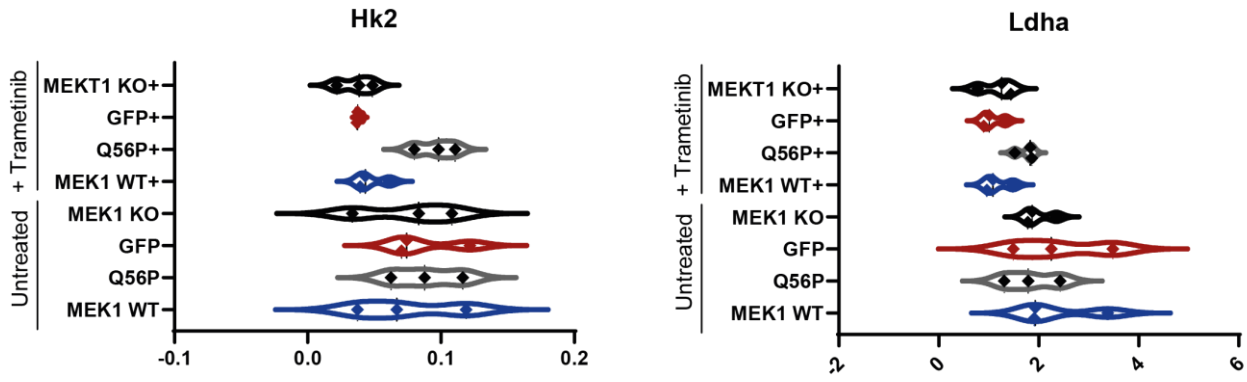

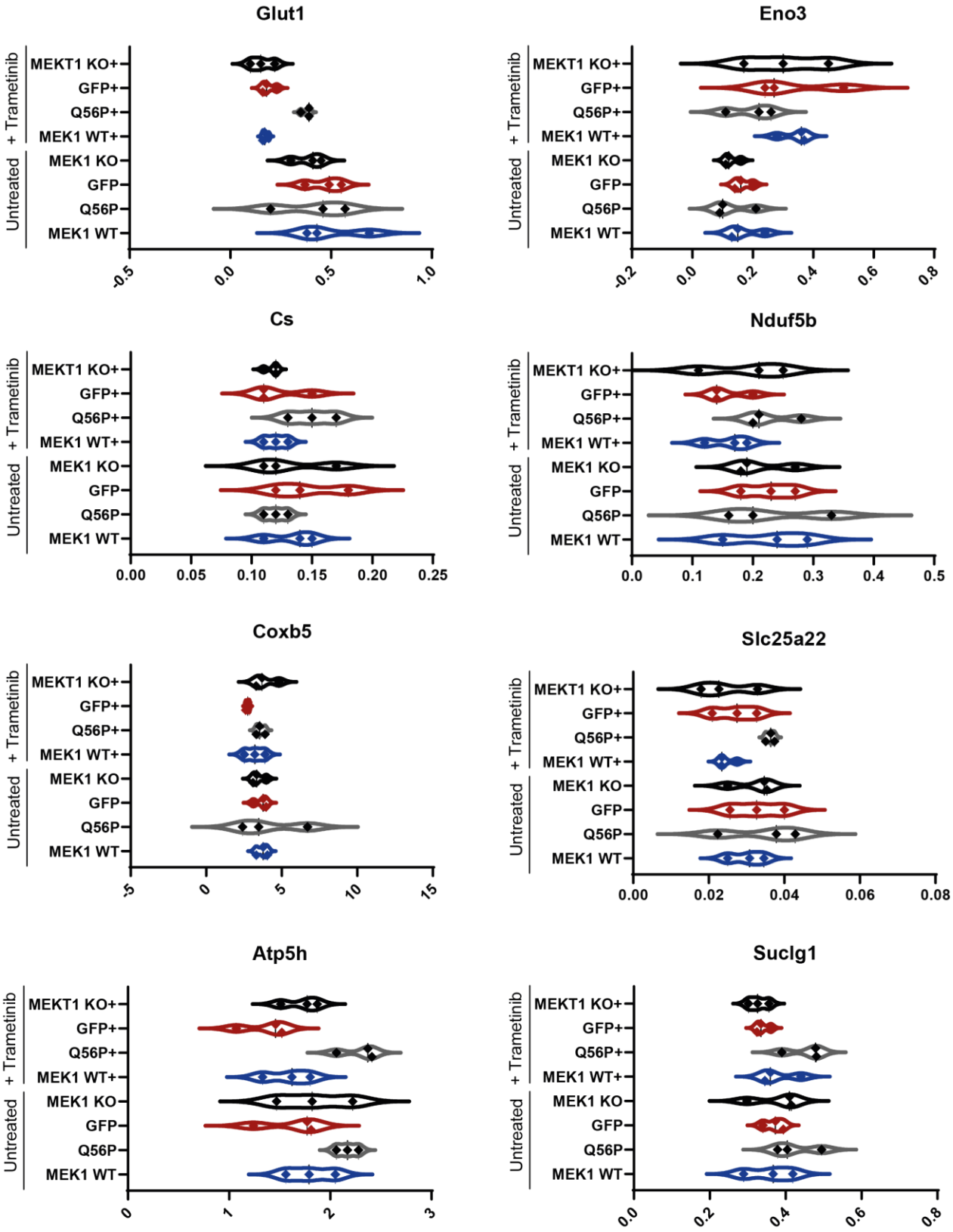
Glut1
Eno3
Cs
Nduf5b
Coxb5
Slc25a22
Atp5h
Suclg1
+ Trametinib
Untreated
MEKT1 KO+
GFP+
Q56P+
MEK1 WT+
MEK1 KO
GFP
Q56P
MEK1 WT

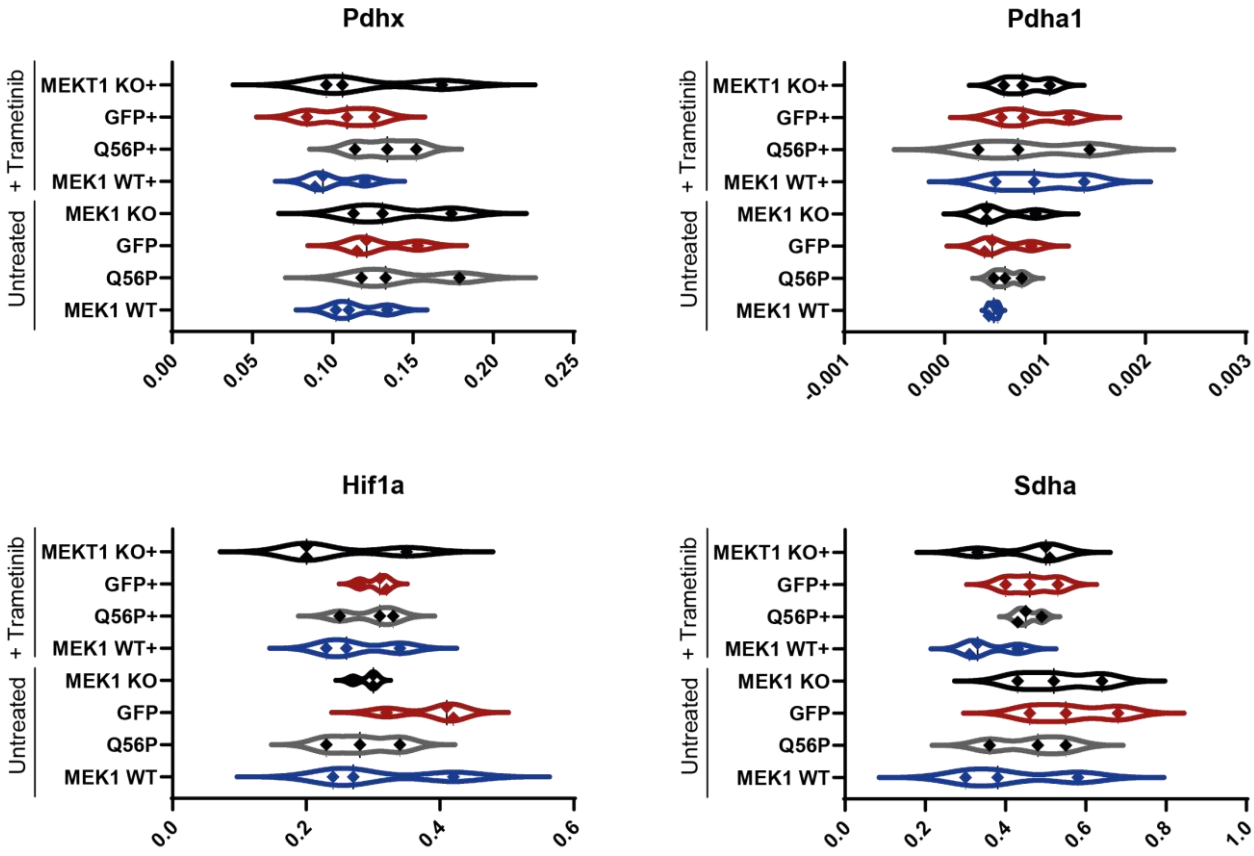

Figure 19 | *Metabolic Gene Expression in Variants of MEK* Violin plots of experimental triplicates indicate the fold change of genes of interest, normalized to housekeeping gene Hprt. MEK1 WT, Q56P, MEK1 KO, and MEK1 KO with a TurboID tagged GFP were investigated under untreated and trametinib treated conditions. While most genes did not show profound difference between genotypes or treatments, Hk2, Ldha, Glut1, and ATP5 did show increased gene expression in Q56P in comparison with the other genotypes.

5.6 Isolation of mitochondria via ultra centrifugation

Based on the data acquired from the PDL screen, we wanted to probe the hypothesis that MEK migrates to the mitochondria, explaining the increase in proximal mitochondrial protein hits observed in the screen. In order to test this, ultracentrifugation was used to isolate mitochondria from MEF cells. The resulting isolation product was probed for MEK, as well as other MAPK components, using western blotting.

Initial mitochondria isolations made use of the abcam mitochondria isolation kit (ab110170). The kit however did not effectively isolate mitochondria in MEF cells. Thus an ultracentrifugation protocol using an OptiPrep gradient was established to try to attain a purer result. Numerous optimization experiments were

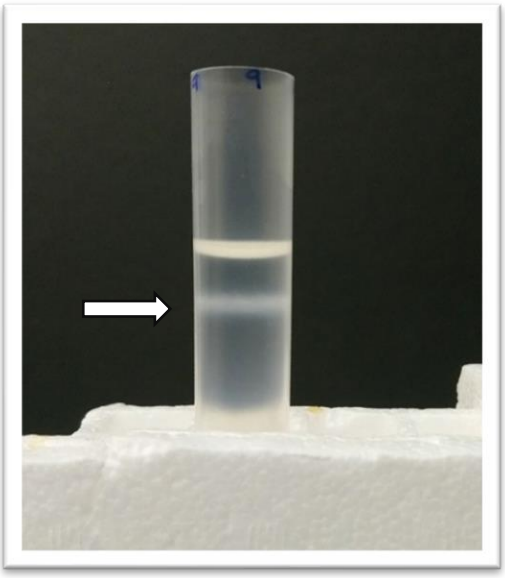

Figure 20 | *Representative OptiPrep™ Gradient Column Post-Ultracentrifugation* After isolation protocol, isolated layer of mitochondria (annotated by arrow) was collected and assessed for purity.

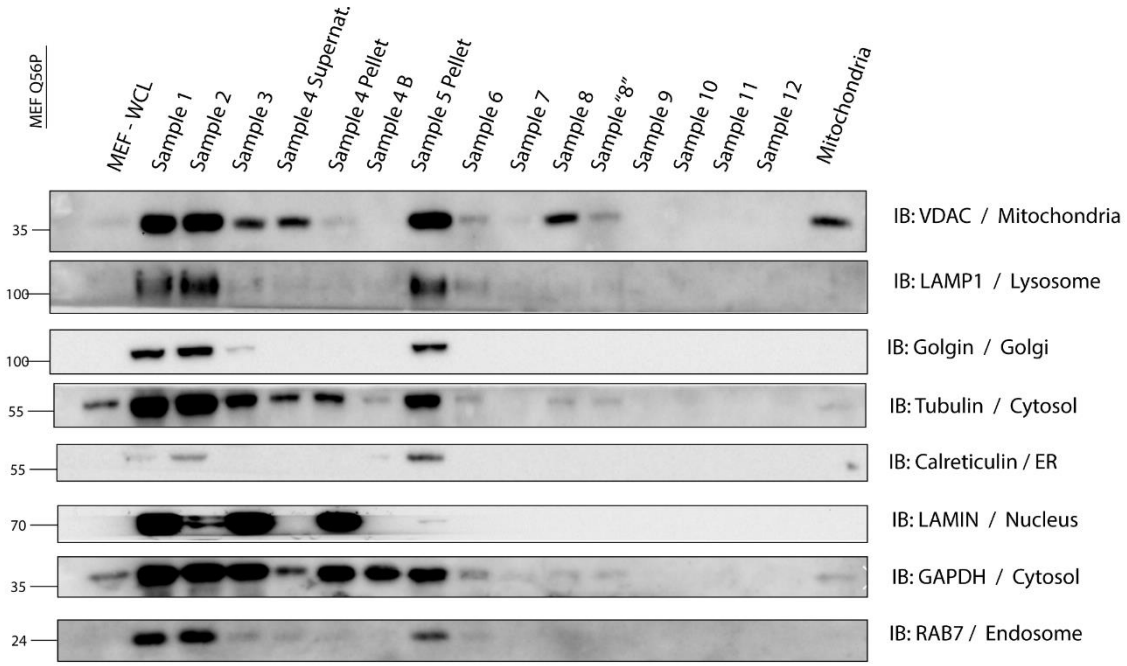

Figure 21 | *Test of Purity post Mitochondria Isolation* Numerous organelle markers were assessed to determine the purity of the mitochondria isolation. The "Sample" numbers refer to samples taken at each step in the protocol, showing purity at each step. "Mitochondria" refers to isolated lysate sample containing majorly mitochondria. Above: Isolation of Q56P. Below: Isolation of MEK1 KO.

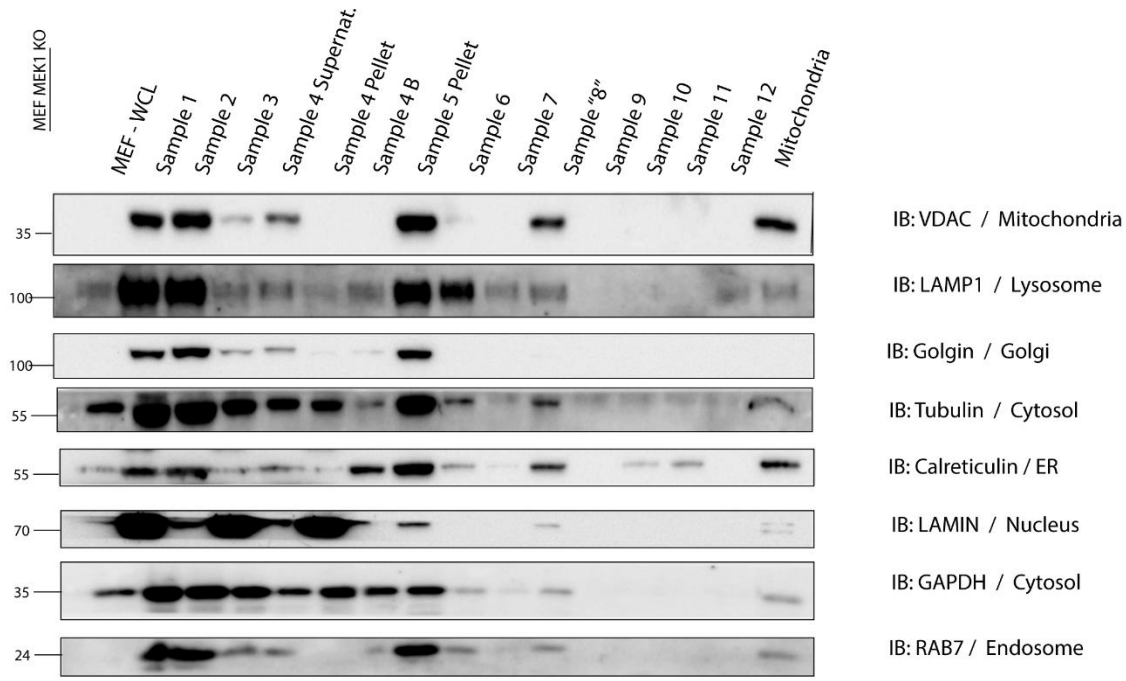

conducted to better the purity of the resulting mitochondria fraction. Samples were taken at each step of the protocol to determine how the experiment could further be optimized. Seen in Figure 21, Sample 1 refers to a dounced whole cell lysate. Sample 5 correlates to a crude mitochondria isolation attained following the numerous dounce steps, but before gradient centrifugation. "Mitochondria" indicates the final product of the centrifugation. Seen in the two exemplary isolations (MEK1 KO & Q56P) variance in purity still arises between fractions, indicating the protocol is still not perfected. However, it is clear in both fractions that mitochondria are significantly enriched (IB: VDAC) compared to other organelles. The endoplasmic reticulum (ER) (IB: Calreticulin) remains the greatest source of contamination, presumably due to the intricate interconnectivity between mitochondria and ER within the cell.

The above isolations were probed for MAPK components, specifically MEK1. Seen in the blots in Figure 22, the Q56P mutant does indicate MEK1 protein content in the mitochondria fraction. This is substantiated through both MEK1 and V5 staining. This result however must not be over interpreted, as contaminations from other cellular compartments (Figure 21) could severely influence this observation. Similarly, other components of the MAPK pathway were observed in the mitochondria fractions of both Q56P and MEK1 KO. Again, because the mitochondria fraction was not perfectly clean, these results cannot conclusively indicate MEK or other components of the MAPK pathway are entering or binding to the mitochondria in the two examined MEK genotypes.

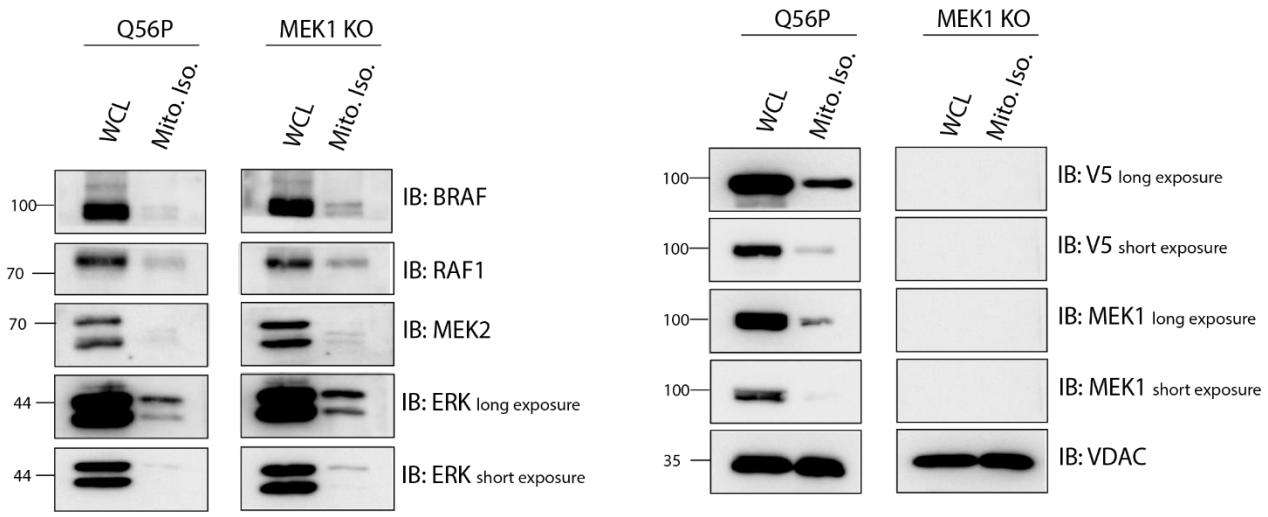

Figure 22 | *Components of MAPK Pathway in Mitochondria Fraction* Western blot assessment of protein content in mitochondria fraction of genotype Q56P and MEK1 KO. WCL represents a dounced whole cell lysate, essentially Sample 1 from *Figure 21.* Mito. Iso. refers to the mitochondria fraction collected post ultracentrifugation and subsequent wash steps.

6. Discussion

Metabolism encompasses a set of essential pathways that provide the energy needed for life. How these pathways are influenced by other critical cellular signaling pathways is a topic that becomes evermore clinically relevant. The link between metabolism and disease has become more evident over the past decades, and enhancing our understanding of this interplay could provide avenues for new treatment options.

This study was inspired by the results of a PDL screen completed by G. Vucak which indicated numerous mitochondria associated proteins in the proximity of MEK1 variants. We had hoped to find a link between MEK1 disease mutations and metabolism. Based on the hits of the screen, we decided to probe different mitochondrial, as well as metabolic, aspects in cells containing specific point mutations of MEK. The Q56P mutant form of MEK1 was our prime candidate for enhanced mitochondria affiliation. The data from this study however implies that the Q56P mutation does not indicate aberrations in mitochondria functionality, or alterations in metabolism when compared to MEK1 WT. Initial Seahorse flux experiments had indicated that the Q56P genotype was associated with reduced maximal OCR compared to MEK1 WT. This initial result made us postulate that the reduced OCR could arise from compromised ETC machinery or alterations in the Micos complex, which is responsible for mitochondria cristae stability. This hypothesis had been in line with the PDL screen data. However, after repeating the Seahorse flux experiments multiple times, we saw that this phenotype was not reproducible. The data, as seen in the above results, indicated that OCR in the Q56P mutant and MEK1 WT was almost identical. We further did not observe any significant differences in mitochondria mass, functionality, or ROS production between MEK1 WT and Q56P.

Proximity dependent labeling using TurboID is reliant on biotinylation of proximal proteins to a bait protein. Mitochondria contain numerous carboxylase enzymes whose function is biotin dependent (Tong, 2013). Because of this, it is known that mitochondrial proteins often arise as false positives in PDL screens. This could explain why we did not observe mitochondria or metabolic differences despite the numerous hits in the PDL screen. Another reason could be the cell type. The PDL screen was conducted in HEK293T cells and the metabolic experiments were carried out in MEF cells. Though both cells express the same variants of MEK1, the cell lines are inherently different in nature. This is exemplified by downstream ERK phosphorylation. The robust ERK activation of the Q56P mutant in HEK293T cells was not observed in MEF cells containing the same mutation. Because of these differences, it could be that the PDL results in HEK293T cells cannot be applied to the fibroblasts.

Differences were however observed between MEK1 WT and MEK1 KO. The loss of MEK1 in MEF cells is associated with an increase in maximal OCR and a consistent decrease in ECAR levels. ECAR correlates to glycolysis, as lactic acid is the main driver of extracellular acidification. Thus the observed drop in ECAR indicates that MEK1 KO has either a decreased rate of glycolysis, or more effectively shuttles pyruvate to the mitochondria for the TCA cycle, reducing the amount of lactic acid produced post-glycolysis. If MEK1 KO MEF cells have increased mitochondria pyruvate uptake, it follows suit that OCR levels in MEK1 KO were also higher. Further experiments would be in order to investigate this hypothesis. Glucose uptake should be measured in the different genotypes and correlated to ECAR. If glucose uptake is also lower in MEK1 KO, it would help justify the claim that MEK1 KO is less glycolytic compared to MEK1 WT. However if glucose uptake was similar in MEK1 KO and MEK1 WT, it would imply that more pyruvate in MEK1 KO is converted to Acetyl-CoA and integrated in the TCA cycle, ultimately leading to less lactic acid production and the observed decrease in ECAR. Our experiments investigating the effects of mitochondrial pyruvate uptake inhibitors showed that max OCR in MEK1 KO was less affected compared to MEK1 WT. As stated, this could indicate MEK1 KO has more non-pyruvate sources for Acetyl-CoA production, perhaps through FAO, or an increase in glutaminolysis. Because the seahorse medium contains only glucose, pyruvate, and glutamate, it seems more likely that MEK1 KO is better able to metabolize glutamate comparatively, leading to the slightly lower decrease in OCR associated with pyruvate uptake inhibition. However, these observations were not statistically significant, merely an observed trend. Thus further replicates are required before any definite statements can be made.

The drop in ECAR observed in MEK1 KO could be induced in MEK1 WT and Q56P via trametinib treatment. Previous studies have also identified impaired glycolysis associated with trametinib treatment (Decroocq et al., 2019). While our results may indicate that the glycolytic shift is MEK dependent, it could also be that by inhibiting or ablating MEK, downstream ERK activity is stunted. It is known that ERK plays a regulatory role in MYC and HIF1α activation. Activated MYC and HIF1α can then regulate glycolysis (Lavoie et al., 2020). However it should be noted that MEK1 WT and Q56P displayed the same shift in ECAR under trametinib treatment. Seen in Figure 18 B, trametinib treatment in Q56P did not inhibit all downstream ERK activation. As such, if this shift were to be ERK dependent, it would be expected that the ECAR shift for MEK1 WT would not mimic the ECAR shift in Q56P. Again however, more experiments are required to define the exact nature of the ECAR shift associated with trametinib treatment.

As we could not conclusively define MEK or other MAPK components in our mitochondria isolations, further experiments are required to determine if MEK in fact enters the mitochondria. Though we did not determine any functional differences associated with the Q56P disease

mutant, it is possible still that Q56P is in the proximity of mitochondria proteins, as indicated in the PDL screen. To determine if Q56P is entering the mitochondria, we had planned to activate the TurboID system, biotinylating proximal proteins, and then perform a mitochondria isolation. If the mitochondria fraction was extremely pure, we could get a biotin readout from the isolation on a wester blot basis. This could imply that MEK is indeed entering the mitochondria. Because of impurities in mitochondria fractionations, we could never get a conclusive result from this experiment. Since the majority of mitochondrial proteins are transcribed in the nucleus and shuttled to the mitochondria, it could be the case that MEK1 is in the proximity of these proteins during their cytosolic journey. This would explain the mitochondria protein hits in the PDL screen and nullify the theory that MEK is entering the mitochondria matrix. Further experiments localizing MEK to these proteins post translation would be required to substantiate this hypothesis.

While we were not able to validate the mitochondria implications of the PDL screen, we were able to show MEK1 ablation increases mitochondria functionality, ROS production and OCR, and decreases ECAR, implying a decrease in glycolysis. We identified that this shift in ECAR was associated with MEK1 ablation and chemical inhibition of MEK. Because ERK activation in MEK1 KO and trametinib treated MEK1 WT were inverse of each other, we believe MEK, not ERK, is the more likely driver of this shift. Metabolism has been described as an Achille's heel in cancer (Kroemer and Pouyssegur, 2008). Deepening our understanding of the interplay between metabolism and signaling pathways associated with cancer will add to the wealth of knowledge required to develop effective, novel therapies.

7. References

Aaronson, S.A., 1991. Growth factors and cancer. Science 254, 1146–1153. https://doi.org/10.1126/science.1659742

Abildgaard, C., Guldberg, P., 2015. Molecular drivers of cellular metabolic reprogramming in melanoma. Trends Mol. Med. 21, 164–171. https://doi.org/10.1016/j.molmed.2014.12.007

Abildgaard, C., Rizza, S., Christiansen, H., Schmidt, S., Dahl, C., Abdul-Al, A., Christensen, A., Filomeni, G., Guldberg, P., 2021. Screening of metabolic modulators identifies new strategies to target metabolic reprogramming in melanoma. Sci. Rep. 11, 4390. https://doi.org/10.1038/s41598-021-83796-8

Barbacid, M., 1987. ras GENES. Annu. Rev. Biochem. 56, 779–827. https://doi.org/10.1146/annurev.bi.56.070187.004023

Berg, J.M., Tymoczko, J.L., Stryer, L., 2002. Biochemistry, 5th Edition. ed.

Bos, J.L., 1989. Review ras Oncogenes in Human Cancer: A Review 9.

Branon, T.C., Bosch, J.A., Sanchez, A.D., Udeshi, N.D., Svinkina, T., Carr, S.A., Feldman, J.L., Perrimon, N., Ting, A.Y., 2018. Efficient proximity labeling in living cells and organisms with TurboID. Nat. Biotechnol. 36, 880–887. https://doi.org/10.1038/nbt.4201

Bromberg-White, J.L., Andersen, N.J., Duesbery, N.S., 2012. MEK genomics in development and disease. Brief. Funct. Genomics 11, 300–310. https://doi.org/10.1093/bfgp/els022

Brunet, A., Pagès, G., Pouysségur, J., 1994. Growth factor-stimulated MAP kinase induces rapid retrophosphorylation and inhibition of MAP kinase kinase (MEK1). FEBS Lett. 346, 299–303. https://doi.org/10.1016/0014-5793(94)00475-7

Buzzai, M., Bauer, D.E., Jones, R.G., Deberardinis, R.J., Hatzivassiliou, G., Elstrom, R.L., Thompson, C.B., 2005. The glucose dependence of Akt-transformed cells can be reversed by pharmacologic activation of fatty acid beta-oxidation. Oncogene 24, 4165–4173. https://doi.org/10.1038/sj.onc.1208622

Cargnello, M., Roux, P.P., 2011. Activation and Function of the MAPKs and Their Substrates, the MAPK-Activated Protein Kinases. Microbiol. Mol. Biol. Rev. 75, 50–83. https://doi.org/10.1128/MMBR.00031-10

Catalanotti, F., Reyes, G., Jesenberger, V., Galabova-Kovacs, G., de Matos Simoes, R., Carugo, O., Baccarini, M., 2009. A Mek1-Mek2 heterodimer determines the strength and duration of the Erk signal. Nat. Struct. Mol. Biol. 16, 294–303. https://doi.org/10.1038/nsmb.1564

Catling, A.D., Reuter, C.W., Cox, M.E., Parsons, S.J., Weber, M.J., 1994. Partial purification of a mitogen-activated protein kinase kinase activator from bovine brain. Identification as B-Raf or a B-Raf-associated activity. J. Biol. Chem. 269, 30014–30021. https://doi.org/10.1016/S0021-9258(18)43982-8

Cheng, Y., Tian, H., 2017. Current Development Status of MEK Inhibitors. Molecules 22, 1551. https://doi.org/10.3390/molecules22101551

Cho, K.F., Branon, T.C., Udeshi, N.D., Myers, S.A., Carr, S.A., Ting, A.Y., 2020. Proximity labeling in mammalian cells with TurboID and split-TurboID. Nat. Protoc. 15, 3971–3999. https://doi.org/10.1038/s41596-020-0399-0

Clarkson, B., Krakoff, I., Burchenal, J., Karnofsky, D., Golbey, R., Dowling, M., Oettgen, H., Lipton, A., 1970. Clinical results of treatment with E. coli L-asparaginase in adults with leukemia, lymphoma, and solid tumors. Cancer 25, 279–305. https://doi.org/10.1002/1097-0142(197002)25:2<279::aid-cncr2820250205>3.0.co;2-7

Collins, R.R.J., Patel, K., Putnam, W.C., Kapur, P., Rakheja, D., 2017. Oncometabolites: A New Paradigm for Oncology, Metabolism, and the Clinical Laboratory. Clin. Chem. 63, 1812–1820. https://doi.org/10.1373/clinchem.2016.267666

Colvin, H., Nishida, N., Konno, M., Haraguchi, N., Takahashi, H., Nishimura, J., Hata, T., Kawamoto, K., Asai, A., Tsunekuni, K., Koseki, J., Mizushima, T., Satoh, T., Doki, Y., Mori, M., Ishii, H., 2016. Oncometabolite D-2-Hydroxyglurate Directly Induces Epithelial-Mesenchymal Transition and is Associated with Distant Metastasis in Colorectal Cancer. Sci. Rep. 6, 1–11. https://doi.org/10.1038/srep36289

Crowley, L.C., Christensen, M.E., Waterhouse, N.J., 2016. Measuring Mitochondrial Transmembrane Potential by TMRE Staining. Cold Spring Harb. Protoc. 2016. https://doi.org/10.1101/pdb.prot087361

Cseh, B., Doma, E., Baccarini, M., 2014. "RAF" neighborhood: Protein–protein interaction in the Raf/Mek/Erk pathway. FEBS Lett., Paris 588, 2398–2406. https://doi.org/10.1016/j.febslet.2014.06.025

DeBerardinis, R.J., Chandel, N.S., 2016. Fundamentals of cancer metabolism. Sci. Adv. 2, e1600200. https://doi.org/10.1126/sciadv.1600200

Decroocq, J., Birsen, R., Mano, J., Fouquet, G., Gotanègre, M., Poulain, L., Mouche, S., Alary, A.-S., Grenier, A., Mazed, F., Mondesir, J., Chapuis, N., Boughalem, A., Le Lorc'h, M., Moura, I.C., Hermine, O., Radford-Weiss, I., Sarry, J.-E., Pasmant, E., Kosmider, O., Bouscary, D., Tamburini, J., 2019. Combination of the MEK Inhibitor Trametinib and Pyrvinium Pamoate Efficiently Targets RAS Pathway-Mutated Acute Myeloid Leukemia in Preclinical Models. Blood 134, 2671–2671. https://doi.org/10.1182/blood-2019-123418

Fowlkes, J.L., Bunn, R.C., Ray, P.D., Kalaitzoglou, E., Uppuganti, S., Unal, M., Nyman, J.S., Thrailkill, K.M., 2020. Constitutive activation of MEK1 in osteoprogenitors increases strength of bone despite impairing mineralization. Bone 130, 115106. https://doi.org/10.1016/j.bone.2019.115106

Ge, T., Yang, J., Zhou, S., Wang, Y., Li, Y., Tong, X., 2020. The Role of the Pentose Phosphate Pathway in Diabetes and Cancer. Front. Endocrinol. 11. https://doi.org/10.3389/fendo.2020.00365

Giroux, S., Tremblay, M., Bernard, D., Cardin-Girard, J.-F., Aubry, S., Larouche, L., Rousseau, S., Huot, J., Landry, J., Jeannotte, L., Charron, J., 1999. Embryonic death of Mek1-deficient mice reveals a role for this kinase in angiogenesis in the labyrinthine region of the placenta. Curr. Biol. 9, 369–376. https://doi.org/10.1016/S0960-9822(99)80164-X

Gonzalez, D., Fearfield, L., Nathan, P., Tanière, P., Wallace, A., Brown, E., Harwood, C., Marsden, J., Whittaker, S., 2013. BRAF mutation testing algorithm for vemurafenib treatment in

melanoma: recommendations from an expert panel. Br. J. Dermatol. 168, 700–707. https://doi.org/10.1111/bjd.12248

Gustafsson, C.M., Falkenberg, M., Larsson, N.-G., 2016. Maintenance and Expression of Mammalian Mitochondrial DNA. Annu. Rev. Biochem. 85, 133–160. https://doi.org/10.1146/annurev-biochem-060815-014402

Guzy, R.D., Hoyos, B., Robin, E., Chen, H., Liu, L., Mansfield, K.D., Simon, M.C., Hammerling, U., Schumacker, P.T., 2005. Mitochondrial complex III is required for hypoxia-induced ROS production and cellular oxygen sensing. Cell Metab. 1, 401–408. https://doi.org/10.1016/j.cmet.2005.05.001

Han, J., Liu, Y., Yang, S., Wu, X., Li, H., Wang, Q., 2021. MEK inhibitors for the treatment of non-small cell lung cancer. J. Hematol. Oncol.J Hematol Oncol 14. https://doi.org/10.1186/s13045-020-01025-7

Harding, A., Hancock, J.F., 2008. Ras nanoclusters: combining digital and analog signaling. Cell Cycle Georget. Tex 7, 127–134. https://doi.org/10.4161/cc.7.2.5237

Hatzivassiliou, G., Song, K., Yen, I., Brandhuber, B.J., Anderson, D.J., Alvarado, R., Ludlam, M.J.C., Stokoe, D., Gloor, S.L., Vigers, G., Morales, T., Aliagas, I., Liu, B., Sideris, S., Hoeflich, K.P., Jaiswal, B.S., Seshagiri, S., Koeppen, H., Belvin, M., Friedman, L.S., Malek, S., 2010. RAF inhibitors prime wild-type RAF to activate the MAPK pathway and enhance growth. Nature 464, 431–435. https://doi.org/10.1038/nature08833

Higgins-Dunn, 2021. Surprise! Amgen's hot KRAS drug seals early FDA approval, winning a shot against "undruggable" cancer [WWW Document]. FiercePharma. URL https://www.fiercepharma.com/pharma/amgen-s-lumakras-becomes-first-fda-approved-kras-inhibitor-for-lung-cancer-patients (accessed 6.1.21).

Hoffner, B., Benchich, K., 2018. Trametinib: A Targeted Therapy in Metastatic Melanoma. J. Adv. Pract. Oncol. 9, 741–745.

Jin, L., Alesi, G.N., Kang, S., 2016. Glutaminolysis as a target for cancer therapy. Oncogene 35, 3619–3625. https://doi.org/10.1038/onc.2015.447

Kaboord, B., Perr, M., 2008. Isolation of proteins and protein complexes by immunoprecipitation. Methods Mol. Biol. Clifton NJ 424, 349–364. https://doi.org/10.1007/978-1-60327-064-9_27

Kang, H., Jha, S., Deng, Z., Fratzl-Zelman, N., Cabral, W.A., Ivovic, A., Meylan, F., Hanson, E.P., Lange, E., Katz, J., Roschger, P., Klaushofer, K., Cowen, E.W., Siegel, R.M., Marini, J.C., Bhattacharyya, T., 2018. Somatic activating mutations in MAP2K1 cause melorheostosis. Nat. Commun. 9. https://doi.org/10.1038/s41467-018-03720-z

Kroemer, G., Pouyssegur, J., 2008. Tumor cell metabolism: cancer's Achilles' heel. Cancer Cell 13, 472–482. https://doi.org/10.1016/j.ccr.2008.05.005

Lam, S.S., Martell, J.D., Kamer, K.J., Deerinck, T.J., Ellisman, M.H., Mootha, V.K., Ting, A.Y., 2015. Directed evolution of APEX2 for electron microscopy and proximity labeling. Nat. Methods 12, 51–54. https://doi.org/10.1038/nmeth.3179

Larsson, N.G., Wang, J., Wilhelmsson, H., Oldfors, A., Rustin, P., Lewandoski, M., Barsh, G.S., Clayton, D.A., 1998. Mitochondrial transcription factor A is necessary for mtDNA maintenance and embryogenesis in mice. Nat. Genet. 18, 231–236. https://doi.org/10.1038/ng0398-231

Laukka, T., Mariani, C.J., Ihantola, T., Cao, J.Z., Hokkanen, J., Kaelin, W.G., Godley, L.A., Koivunen, P., 2016. Fumarate and Succinate Regulate Expression of Hypoxia-inducible Genes via TET Enzymes. J. Biol. Chem. 291, 4256–4265. https://doi.org/10.1074/jbc.M115.688762

Lavoie, H., Gagnon, J., Therrien, M., 2020. ERK signalling: a master regulator of cell behaviour, life and fate. Nat. Rev. Mol. Cell Biol. 21, 607–632. https://doi.org/10.1038/s41580-020-0255-7

Lemmon, M.A., Schlessinger, J., 2010. Cell Signaling by Receptor Tyrosine Kinases. Cell 141, 1117–1134. https://doi.org/10.1016/j.cell.2010.06.011

Li, F., Wang, Y., Zeller, K.I., Potter, J.J., Wonsey, D.R., O'Donnell, K.A., Kim, J.-W., Yustein, J.T., Lee, L.A., Dang, C.V., 2005. Myc stimulates nuclearly encoded mitochondrial genes and mitochondrial biogenesis. Mol. Cell. Biol. 25, 6225–6234. https://doi.org/10.1128/MCB.25.14.6225-6234.2005

Little, A.C., Kovalenko, I., Goo, L.E., Hong, H.S., Kerk, S.A., Yates, J.A., Purohit, V., Lombard, D.B., Merajver, S.D., Lyssiotis, C.A., 2020. High-content fluorescence imaging with the metabolic flux assay reveals insights into mitochondrial properties and functions. Commun. Biol. 3, 1–10. https://doi.org/10.1038/s42003-020-0988-z

Liu, Y., Gray, N.S., 2006. Rational design of inhibitors that bind to inactive kinase conformations. Nat. Chem. Biol. 2, 358–364. https://doi.org/10.1038/nchembio799

Lobingier, B.T., Hüttenhain, R., Eichel, K., Miller, K.B., Ting, A.Y., von Zastrow, M., Krogan, N.J., 2017. An Approach to Spatiotemporally Resolve Protein Interaction Networks in Living Cells. Cell 169, 350-360.e12. https://doi.org/10.1016/j.cell.2017.03.022

Long, G.V., Menzies, A.M., Nagrial, A.M., Haydu, L.E., Hamilton, A.L., Mann, G.J., Hughes, T.M., Thompson, J.F., Scolyer, R.A., Kefford, R.F., 2011. Prognostic and Clinicopathologic Associations of Oncogenic BRAF in Metastatic Melanoma. J. Clin. Oncol. 29, 1239–1246. https://doi.org/10.1200/JCO.2010.32.4327

Loschen, G., Azzi, A., Richter, C., Flohé, L., 1974. Superoxide radicals as precursors of mitochondrial hydrogen peroxide. FEBS Lett. 42, 68–72. https://doi.org/10.1016/0014-5793(74)80281-4

Lugowska, I., Koseła-Paterczyk, H., Kozak, K., Rutkowski, P., 2015. Trametinib: a MEK inhibitor for management of metastatic melanoma. OncoTargets Ther. 8, 2251–2259. https://doi.org/10.2147/OTT.S72951

Mankoff, D.A., Eary, J.F., Link, J.M., Muzi, M., Rajendran, J.G., Spence, A.M., Krohn, K.A., 2007. Tumor-specific positron emission tomography imaging in patients: [18F] fluorodeoxyglucose and beyond. Clin. Cancer Res. Off. J. Am. Assoc. Cancer Res. 13, 3460–3469. https://doi.org/10.1158/1078-0432.CCR-07-0074

Marks, J.L., Gong, Y., Chitale, D., Golas, B., McLellan, M.D., Kasai, Y., Ding, L., Mardis, E.R., Wilson, R.K., Solit, D., Levine, R., Michel, K., Thomas, R.K., Rusch, V.W., Ladanyi, M., Pao, W., 2008. Novel MEK1 Mutation Identified by Mutational Analysis of Epidermal Growth Factor

Receptor Signaling Pathway Genes in Lung Adenocarcinoma. Cancer Res. 68, 5524–5528. https://doi.org/10.1158/0008-5472.CAN-08-0099

Marshall, C.J., 1995. Specificity of receptor tyrosine kinase signaling: Transient versus sustained extracellular signal-regulated kinase activation. Cell 80, 179–185. https://doi.org/10.1016/0092-8674(95)90401-8

Mitochondrial Disease | UMDF, n.d. URL https://www.umdf.org/what-is-mitochondrial-disease-2/ (accessed 6.20.21).

Murphy, M.P., 2009. How mitochondria produce reactive oxygen species. Biochem. J. 417, 1–13. https://doi.org/10.1042/BJ20081386

Murugan, A.K., Dong, J., Xie, J., Xing, M., 2009. MEK1 mutations, but not ERK2 mutations, occur in melanomas and colon carcinomas, but none in thyroid carcinomas. Cell Cycle Georget. Tex 8, 2122–2124. https://doi.org/10.4161/cc.8.13.8710

Nelson, D., 2017. Lehninger Principles of Biochemistry, 4th ed. New York: Worth Publishers.

Nichols, R.J., Haderk, F., Stahlhut, C., Schulze, C.J., Hemmati, G., Wildes, D., Tzitzilonis, C., Mordec, K., Marquez, A., Romero, J., Hsieh, T., Zaman, A., Olivas, V., McCoach, C., Blakely, C.M., Wang, Z., Kiss, G., Koltun, E.S., Gill, A.L., Singh, M., Goldsmith, M.A., Smith, J.A.M., Bivona, T.G., 2018. RAS nucleotide cycling underlies the SHP2 phosphatase dependence of mutant BRAF-, NF1- and RAS-driven cancers. Nat. Cell Biol. 20, 1064–1073. https://doi.org/10.1038/s41556-018-0169-1

Ohren, J.F., Chen, H., Pavlovsky, A., Whitehead, C., Zhang, E., Kuffa, P., Yan, C., McConnell, P., Spessard, C., Banotai, C., Mueller, W.T., Delaney, A., Omer, C., Sebolt-Leopold, J., Dudley, D.T., Leung, I.K., Flamme, C., Warmus, J., Kaufman, M., Barrett, S., Tecle, H., Hasemann, C.A., 2004. Structures of human MAP kinase kinase 1 (MEK1) and MEK2 describe novel noncompetitive kinase inhibition. Nat. Struct. Mol. Biol. 11, 1192–1197. https://doi.org/10.1038/nsmb859

Prior, I.A., Lewis, P.D., Mattos, C., 2012. A Comprehensive Survey of Ras Mutations in Cancer. Cancer Res. 72, 2457–2467. https://doi.org/10.1158/0008-5472.CAN-11-2612

Qin, W., Cho, K.F., Cavanagh, P.E., Ting, A.Y., 2021. Deciphering molecular interactions by proximity labeling. Nat. Methods 18, 133–143. https://doi.org/10.1038/s41592-020-01010-5

Reddy, B.P., Khadgapathi, P., Tiwari, D.S., Kumar, K.A., 2017. Pharmaceutical compositions of trametinib. US20170020880A1.

Roskoski, R., 2012. MEK1/2 dual-specificity protein kinases: Structure and regulation. Biochem. Biophys. Res. Commun. 417, 5–10. https://doi.org/10.1016/j.bbrc.2011.11.145

Rossomando, A.J., Dent, P., Sturgill, T.W., Marshak, D.R., 1994. Mitogen-activated protein kinase kinase 1 (MKK1) is negatively regulated by threonine phosphorylation. Mol. Cell. Biol. 14, 1594–1602. https://doi.org/10.1128/mcb.14.3.1594

Roux, K.J., Kim, D.I., Raida, M., Burke, B., 2012. A promiscuous biotin ligase fusion protein identifies proximal and interacting proteins in mammalian cells. J. Cell Biol. 196, 801–810. https://doi.org/10.1083/jcb.201112098

Ryan, M.B., Corcoran, R.B., 2018. Therapeutic strategies to target RAS-mutant cancers. Nat. Rev. Clin. Oncol. 15, 709–720. https://doi.org/10.1038/s41571-018-0105-0

Sabharwal, S.S., Schumacker, P.T., 2014. Mitochondrial ROS in cancer: initiators, amplifiers or an Achilles' heel? Nat. Rev. Cancer 14, 709–721. https://doi.org/10.1038/nrc3803

Schadendorf, D., Amonkar, M.M., Milhem, M., Grotzinger, K., Demidov, L.V., Rutkowski, P., Garbe, C., Dummer, R., Hassel, J.C., Wolter, P., Mohr, P., Trefzer, U., Lefeuvre-Plesse, C., Rutten, A., Steven, N., Ullenhag, G., Sherman, L., Wu, F.S., Patel, K., Casey, M., Robert, C., 2014. Functional and symptom impact of trametinib versus chemotherapy in BRAF V600E advanced or metastatic melanoma: quality-of-life analyses of the METRIC study. Ann. Oncol. 25, 700–706. https://doi.org/10.1093/annonc/mdt580

Scholl, F.A., Dumesic, P.A., Barragan, D.I., Harada, K., Bissonauth, V., Charron, J., Khavari, P.A., 2007. Mek1/2 MAPK Kinases Are Essential for Mammalian Development, Homeostasis, and Raf-Induced Hyperplasia. Dev. Cell 12, 615–629. https://doi.org/10.1016/j.devcel.2007.03.009

Sebolt-Leopold, J.S., Herrera, R., 2004. Targeting the mitogen-activated protein kinase cascade to treat cancer. Nat. Rev. Cancer 4, 937–947. https://doi.org/10.1038/nrc1503

Selvasaravanan, K.D., Wiederspohn, N., Hadzalic, A., Strobel, H., Payer, C., Schuster, A., Karpel-Massler, G., Siegelin, M.D., Halatsch, M.-E., Debatin, K.-M., Westhoff, M.-A., 2020. The limitations of targeting MEK signalling in Glioblastoma therapy. Sci. Rep. 10, 7401. https://doi.org/10.1038/s41598-020-64289-6

Semenza, G.L., 2003. Targeting HIF-1 for cancer therapy. Nat. Rev. Cancer 3, 721–732. https://doi.org/10.1038/nrc1187

Serasinghe, M.N., Gelles, J.D., Li, K., Zhao, L., Abbate, F., Syku, M., Mohammed, J.N., Badal, B., Rangel, C.A., Hoehn, K.L., Celebi, J.T., Chipuk, J.E., 2018. Dual suppression of inner and outer mitochondrial membrane functions augments apoptotic responses to oncogenic MAPK inhibition. Cell Death Dis. 9, 1–13. https://doi.org/10.1038/s41419-017-0044-1

Sickmann, A., Reinders, J., Wagner, Y., Joppich, C., Zahedi, R., Meyer, H.E., Schönfisch, B., Perschil, I., Chacinska, A., Guiard, B., Rehling, P., Pfanner, N., Meisinger, C., 2003. The proteome of Saccharomyces cerevisiae mitochondria. Proc. Natl. Acad. Sci. U. S. A. 100, 13207–13212. https://doi.org/10.1073/pnas.2135385100

Slack-Davis, J.K., Eblen, S.T., Zecevic, M., Boerner, S.A., Tarcsafalvi, A., Diaz, H.B., Marshall, M.S., Weber, M.J., Parsons, J.T., Catling, A.D., 2003. PAK1 phosphorylation of MEK1 regulates fibronectin-stimulated MAPK activation. J. Cell Biol. 162, 281–291. https://doi.org/10.1083/jcb.200212141

Tong, L., 2013. Structure and function of biotin-dependent carboxylases. Cell. Mol. Life Sci. CMLS 70, 863–891. https://doi.org/10.1007/s00018-012-1096-0

Trunzer, K., Pavlick, A.C., Schuchter, L., Gonzalez, R., McArthur, G.A., Hutson, T.E., Moschos, S.J., Flaherty, K.T., Kim, K.B., Weber, J.S., Hersey, P., Long, G.V., Lawrence, D., Ott, P.A., Amaravadi, R.K., Lewis, K.D., Puzanov, I., Lo, R.S., Koehler, A., Kockx, M., Spleiss, O., Schell-Steven, A., Gilbert, H.N., Cockey, L., Bollag, G., Lee, R.J., Joe, A.K., Sosman, J.A., Ribas, A., 2013. Pharmacodynamic effects and mechanisms of resistance to vemurafenib in patients

with metastatic melanoma. J. Clin. Oncol. Off. J. Am. Soc. Clin. Oncol. 31, 1767–1774. https://doi.org/10.1200/JCO.2012.44.7888

Warburg, O., 1956. On the Origin of Cancer Cells. Science 123, 309–314. https://doi.org/10.1126/science.123.3191.309

Warburg, O., 1925. The Metabolism of Carcinoma Cells. J. Cancer Res. 9, 148–163. https://doi.org/10.1158/jcr.1925.148

Ward, P.S., Thompson, C.B., 2012. Metabolic Reprogramming: A Cancer Hallmark Even Warburg Did Not Anticipate. Cancer Cell 21, 297–308. https://doi.org/10.1016/j.ccr.2012.02.014

Waterfall, J.J., Arons, E., Walker, R.L., Pineda, M., Roth, L., Killian, J.K., Abaan, O.D., Davis, S.R., Kreitman, R.J., Meltzer, P.S., 2014. High prevalence of MAP2K1 mutations in variant and IGHV4-34 expressing hairy-cell leukemia. Nat. Genet. 46, 8–10. https://doi.org/10.1038/ng.2828

Weber, P.C., Ohlendorf, D.H., Wendoloski, J.J., Salemme, F.R., 1989. Structural origins of high-affinity biotin binding to streptavidin. Science 243, 85–88. https://doi.org/10.1126/science.2911722

Weinberg, F., Hamanaka, R., Wheaton, W.W., Weinberg, S., Joseph, J., Lopez, M., Kalyanaraman, B., Mutlu, G.M., Budinger, G.R.S., Chandel, N.S., 2010. Mitochondrial metabolism and ROS generation are essential for Kras-mediated tumorigenicity. Proc. Natl. Acad. Sci. 107, 8788–8793.

Wellbrock, C., Karasarides, M., Marais, R., 2004. The RAF proteins take centre stage. Nat. Rev. Mol. Cell Biol. 5, 875–885. https://doi.org/10.1038/nrm1498

Wetzker, R., Böhmer, F.-D., 2003. Transactivation joins multiple tracks to the ERK/MAPK cascade. Nat. Rev. Mol. Cell Biol. 4, 651–657. https://doi.org/10.1038/nrm1173

Wise, D.R., DeBerardinis, R.J., Mancuso, A., Sayed, N., Zhang, X.-Y., Pfeiffer, H.K., Nissim, I., Daikhin, E., Yudkoff, M., McMahon, S.B., Thompson, C.B., 2008. Myc regulates a transcriptional program that stimulates mitochondrial glutaminolysis and leads to glutamine addiction. Proc. Natl. Acad. Sci. U. S. A. 105, 18782–18787. https://doi.org/10.1073/pnas.0810199105

Wong, K.K.L., Liao, J.Z., Shih, C.R.Y., Harden, N., Verheyen, E.M., 2020. Hyperpolarized mitochondria accumulate in Drosophila Hipk-overexpressing cells to drive tumor-like growth. J. Cell Sci. 133. https://doi.org/10.1242/jcs.250944

Yang, M., Soga, T., Pollard, P.J., 2013. Oncometabolites: linking altered metabolism with cancer. J. Clin. Invest. 123, 3652–3658. https://doi.org/10.1172/JCI67228

Zhao, Y., Adjei, A.A., 2014. The clinical development of MEK inhibitors. Nat. Rev. Clin. Oncol. 11, 385–400. https://doi.org/10.1038/nrclinonc.2014.83

ZHENG, J., 2012. Energy metabolism of cancer: Glycolysis versus oxidative phosphorylation (Review). Oncol. Lett. 4, 1151–1157. https://doi.org/10.3892/ol.2012.928

Zhou, W., Zhang, Y., Hosch, M.S., Lang, A., Zwacka, R.M., Engelhardt, J.F., 2001. Subcellular site of superoxide dismutase expression differentially controls AP-1 activity and injury in mouse liver following ischemia/reperfusion. Hepatol. Baltim. Md 33, 902–914. https://doi.org/10.1053/jhep.2001.23073